

Induced pluripotent stem cells (iPSCs) are pluripotent cell lines directly reprogrammed from somatic cells.¹⁷ Patient-derived iPSCs can provide somatic cells, which cannot be directly obtained from patients, and this discovery has led to the development of a new field of disease modeling (reviewed by Grskovic et al¹⁸). In addition, iPSC technology has another interesting characteristic that each iPSC clone originates from a single cell,¹⁹ which may make it possible to obtain genetically different iPSC clones from a person.

In this study, we established mutant and nonmutant iPSC lines from the same patients by deriving iPSCs from patients carrying a mutation of an autosomal gene as somatic mosaicism. By analyzing the disease-relevant characteristic of IL-1 β secretion, we demonstrated that mutant macrophages are mainly responsible for the disease phenotype in the mosaic patients. Moreover, using a robust differentiation protocol to generate macrophages and purifying them by their surface marker expression, we showed that drug candidates inhibit the IL-1 β secretion from mutant macrophages. Our data prove the usefulness of iPSC technology both for dissecting somatic mosaicism and as a platform for drug discovery of multiple NLRP3-related inflammatory diseases.

Methods

Human iPSC generation

We obtained skin biopsy specimens from 2 independent patients (patient 1, CIRA188Ai; and patient 2, CIRA086Ai). This study was approved by Ethics Committee of Kyoto University, and informed consent was obtained from both the patients and their guardians in accordance with the Declaration of Helsinki. We expanded the fibroblasts in DMEM (Nacalai Tesque) containing 10% FBS (Invitrogen) and 0.5% penicillin and streptomycin (Invitrogen). Generation of iPSCs was performed as described previously.¹⁷ In brief, we introduced *OCT3/4*, *SOX2*, *KLF4*, and *c-MYC* using ecotropic retroviral transduction into fibroblasts expressing the mouse *Slc7a1* gene. Six days after transduction, the cells were harvested and replated onto mitotically inactivated SNL feeder cells. The next day, we replaced the medium with Primate ES cell medium (ReproCELL) supplemented with 4 ng/mL bFGF (Wako). Three weeks after this period, individual colonies were isolated and expanded. Cell culture was performed under 37°C, with 5% CO₂ and 21% O₂ unless otherwise stated. Cells were examined using Olympus CKX41 inverted microscope equipped with Nikon Digital Sight DS-L2 camera. A UPlan FLN 4 \times /0.13 objective (Nikon) was used for image acquisition.

Genetic analysis

Genomic DNA from either fibroblasts or iPSCs was isolated. The PCR product of exon 3 of *NLRP3* was sequenced directly or after subcloning with a TOPO TA cloning kit (Invitrogen), using an ABI 3100 sequencer (Applied Biosystems). For pyrosequencing, the PCR product of exon 3 of *NLRP3* was analyzed by PyroMarkQ96ID (QIAGEN).

RNA isolation and quantitative PCR for *NANOG* and the transgene

Total RNA was purified with the Trizol reagent (Invitrogen) and treated with a Turbo DNA-free kit (Ambion) to remove genomic DNA contamination. A total of 1 μ g of total RNA was used for a reverse transcription reaction with ReverTraAce- α (Toyobo) and the dT₂₀ primer, according to the manufacturer's instructions. Quantitative PCR was performed on the 7900HT Fast Real-Time PCR System (Applied Biosystems) with SYBR Premix ExTaqII (Takara). The primer sequences are described in supplemental Table 4 (available on the *Blood* Web site; see the Supplemental Materials link at the top of the online article).

Southern blotting

Genomic DNA (5 μ g) was digested with BglIII and ScaI overnight. The digested DNA fragments were separated on 1% agarose gels and were transferred to a nylon membrane (GE Healthcare). The membrane was incubated with a digoxigenin (DIG)-labeled human *cMYC* DNA probe in DIG Easy Hyb buffer (Roche Diagnostics) at 42°C overnight with constant agitation. After washing, an alkaline phosphatase-conjugated anti-DIG antibody (1:10 000; Roche Diagnostics) was added to a membrane. Signals were obtained using CDP-star (Roche Diagnostics) and detected by an LAS4000 imaging system.

Teratoma formation

Approximately 2×10^6 cells were injected subcutaneously into the dorsal flank of immunocompromised NOD/scid/ γ c^{null} mice (Central Institute for Experimental Animals). Masses were excised 8 to 10 weeks after injection and fixed with PBS containing 4% paraformaldehyde. Paraffin-embedded tissues were sliced and stained with hematoxylin and eosin. Slides were examined using BIOREVO BZ-9000 (KEYENCE). A PlanApo 20 \times /0.75 objective (Nikon) and BZ-II Viewer software (KEYENCE) were used for image acquisition.

In vitro differentiation into macrophages

Undifferentiated human embryonic stem cell (ESC) and iPSC lines were cultured on mitotically inactivated SNL feeder cells with Primate ES cell medium supplemented with 4 ng/mL bFGF. During the differentiation of the cells into macrophages, cells were cultured under 37°C, with 5% CO₂ and 5% O₂. On day 0, the iPSCs were plated at a ratio of 1:15 onto a mitotically inactivated OP9 feeder layer on 100-mm cell culture plates in α -MEM (Invitrogen) containing 10% FBS and 1% Antibiotic-Antimycotic (Invitrogen) supplemented with 50 ng/mL VEGF α (R&D Systems). On day 5, the medium was changed. On day 10, the differentiating iPSCs were collected by trypsinization, and Tra-1-85⁺ CD34⁺ and KDR⁺ hematopoietic progenitors were sorted on a FACSAria II instrument (BD Biosciences). The progenitors were plated at 2×10^4 cells on another mitotically inactivated OP9 feeder layer on 100-mm cell culture plates or at 3×10^3 cells/well in 6-well cell culture plates in α -MEM containing 10% FBS and 1% Antibiotic-Antimycotic supplemented with 50 ng/mL IL-3, 50 ng/mL stem cell factor, 10 ng/mL thrombopoietin, 50 ng/mL Flt-3 ligand, and 50 ng/mL M-CSF (all R&D Systems). On day 18, the medium was changed. On day 26, differentiating cells were collected with Accumax (Innovative Cell Technologies), and CD14⁺ iPSC-derived macrophages were purified on an autoMACSpro instrument (Miltenyi Biotec).

Peripheral blood mononuclear cells (PBs) were obtained from healthy volunteers, and CD14⁺ monocytes were purified on the autoMACSpro instrument. For macrophage differentiation, 5×10^5 monocytes were plated in 6-well cell culture plates in RPMI 1640 (Sigma-Aldrich) containing 10% FBS and 1% Antibiotic-Antimycotic supplemented with 50 ng/mL M-CSF. On day 5, the adherent cells were collected with Accumax, and CD14⁺ blood-derived macrophages (B-MPs) were purified on the autoMACSpro instrument. May-Giemsa-stained slides were examined using BIOREVO BZ-9000. A PlanApo 40 \times /0.95 objective (Nikon) and BZ-II Viewer software were used for image acquisition.

FACS analysis

Hematopoietic marker expression was evaluated on a MACSQuant Analyzer (Miltenyi Biotec). Primary antibodies Tra-1-85-FITC (R&D Systems), CD34-PE (Beckman Coulter), KDR-AlexaFluor-647 (BioLegend), CD45-PE (BD Biosciences PharMingen), and CD14-APC (Beckman Coulter) were used.

Immunocytochemistry

For immunocytochemistry, cells were fixed with PBS containing 4% paraformaldehyde for 5 minutes, permeabilized in PBS containing 0.1% Tween 20 for 5 minutes, and blocked in PBS containing 3% BSA for 10 minutes, all at room temperature. The primary antibody was for CD68 (1:50; Santa Cruz Biotechnology), and the secondary antibody was Cy3-conjugated

AffiniPure Donkey Anti-Mouse IgG (1:100; Jackson ImmunoResearch Laboratories). Nuclei were stained with 1 $\mu\text{g}/\text{mL}$ Hoechst 33342 (Invitrogen). Cells were examined using BIOREVO BZ-9000. A Plan Fluor DL 10 \times /0.30 Ph1 objective (Nikon) and BZ-II Viewer software were used for image acquisition.

Electron microscopy

The 5×10^4 macrophages in 20 μL suspension were placed on the poly-L-lysine treated, carbon-coated sapphire disks (3 mm in diameter) and incubated for 30 minutes at 37°C with 5% CO₂. The cell-adsorbed disk was then subjected to chemical fixation with 2.5% glutaraldehyde in NaHCO₃ buffer (100mM NaCl, 30mM HEPES, 2mM CaCl₂, adjusted at pH 7.4 with NaOH). These specimens were postfixed with 1% osmium and 1.5% K₄Fe(CN)₆ in 0.1M PBS buffer, washed, dehydrated with a series of ethanol, and embedded in Epoxy resin (TAAB EPO812). After the polymerization at 70°C, the ultra-sections (70 nm) obtained by Ultramicrotome (Leica FC6) were mounted in EM grids, stained with uranyl acetate/lead citrate, and then observed by conventional TEM (JEOL JEM1400).

PCR and microarray analysis of macrophages

Total RNA was column-purified with the RNeasy kit (QIAGEN) and treated with RNase-free DNase (QIAGEN). A total of 20 ng of total RNA was reverse transcribed into cDNA using random primers and the Sensiscript RT Kit (QIAGEN). Quantitative PCR was performed on a StepOne Plus Real-Time PCR System (Applied Biosystems) with TaqMan Gene Expression Master Mix (Applied Biosystems). The primer sequences are described in supplemental Table 4. For the microarray analysis, RNA probes were hybridized to SurePrint G3 Human GE 8 \times 60K Microarrays (Agilent Technologies) according to the manufacturer's protocols. Microarrays were scanned, and the data were analyzed using the GeneSpring GX Version 11 software program (Agilent Technologies). The complete dataset from this analysis is available at the NCBI Gene Expression Omnibus using accession no. GSE38626.

LM infection

Listeria monocytogenes EGD (LM) were grown in brain heart infusion broth (Eieken Chemical), washed, suspended in PBS supplemented with 10% glycerol, and stored in aliquots at -80°C . Macrophages were seeded into an 8-well chamber slide at 2×10^5 cells/well in RPMI containing 10% FBS and then infected with bacteria at a multiplicity of infection of 10 for 60 minutes at 37°C. Cells were cultured for further 1 or 5 hours in the presence of 5 $\mu\text{g}/\text{mL}$ gentamicin. The cells were fixed in 4% paraformaldehyde and incubated with PBS containing 10% Blocking One (Nacalai Tesque) and 0.1% saponin. F-actin and nuclei were visualized by staining with Alexa-488-phalloidin (Invitrogen) and 4',6-diamidino-2-phenylindole (Dojindo), respectively. The bacteria were stained by treatment with a goat anti-*Listeria* polyclonal antibody (Kirkegaard & Perry Laboratories) and then with the Alexa 546 anti-goat IgG antibody (Invitrogen). Slides were examined using BIOREVO BZ-9000. A PlanApo_VC 100 \times /H1.40 objective (Nikon) and BZ-II Viewer software were used for image acquisition, and BZ-II Analyzer (KEYENCE) was used for image processing. Immunofluorescence was evaluated with the IN Cell Analyzer 2000, and samples were analyzed with the IN Cell Developer Toolbox Version 1.8 software program (GE Healthcare).

Cytokine secretion from macrophages

Purified iPSC-MPs or B-MPs were seeded at the indicated counts per well or 5×10^4 cells/well unless otherwise stated in 96-well cell culture plates in RPMI 1640 containing 10% FBS and 1% Antibiotic-Antimycotic. Cells were cultured for 2 hours in the presence or absence of inhibitors. The plates were centrifuged at 300g for 10 minutes; then the medium was changed. Cells were cultured for 4 hours in the presence of LPS or recombinant human IL-1 β . LPS concentration was 1 $\mu\text{g}/\text{mL}$ unless otherwise stated. After the 30 minute or 1-hour culture after the addition of 1mM ATP (Sigma-Aldrich), we collected the supernatants and cell lysates. As second

signal stimulants, we also used 500 $\mu\text{g}/\text{mL}$ silica crystals (U.S. silica) for 1 hour, or 100 $\mu\text{g}/\text{mL}$ monosodium urate crystals (Sigma-Aldrich) for 3 hours. For the supernatant transfer experiments, we harvested the supernatant from the wells of mutant or wild-type iPSC-MPs, which were stimulated with LPS for 4 hours. After centrifugation, we transferred the supernatants to the wells of other iPSC-MPs and cultured them for another 4 hours. The cytokine concentration of the supernatants was determined using a Th1/Th2 11plex FlowCytomix Kit (Bender MedSystems) following the manufacturer's instructions. Reagents were purchased as follows: CA074Me (Calbiochem), IL-1Ra (R&D Systems), oxidized ATP (oATP; Sigma-Aldrich), pyridoxalphosphate-6-azophenyl-2',4'-disulphonic acid (PPADS; Sigma-Aldrich), cycloheximide (Sigma-Aldrich), MG132 (Calbiochem), Bay11-7082 (Sigma-Aldrich), and Ac-YVAD-CHO (Calbiochem).

LDH secretion assay

The lactate dehydrogenase (LDH) concentration of the supernatants of iPSC-MPs after a 4-hour culture with LPS was determined with an LDH Cytotoxicity Detection kit (Takara) following the manufacturer's instructions.

Statistical analysis

The data were processed using the SPSS Statistics Version 18 software package. The values are reported as the mean \pm SEM. Comparisons between groups were performed using the unpaired Student *t* test. *P* < .05 was considered statistically significant.

Results

Establishment and characterization of iPSCs

Dermal fibroblasts were obtained from 2 male CINCA patients who had mutations of *NLRP3* as somatic mosaicism. Both patients had nonsynonymous point mutations in the *NLRP3* coding region. The fibroblasts from patients 1 and 2 contained 34% and 9.8% mutant cells, respectively (Figure 1A; supplemental Figure 1A). These fibroblasts were reprogrammed to iPSCs after transduction with retroviral vectors encoding *OCT3/4*, *SOX2*, *KLF4*, and *cMYC*.¹⁷ Twelve of the 28 isolated clones from patient 1, and 3 of 30 clones from patient 2 had a heterozygous mutation of the *NLRP3* gene, whereas the rest of the clones were wild-type (Figure 1A; supplemental Figure 1B-C). The frequency of mutants was comparable among blood cells,^{9,20} fibroblasts, and iPSCs (Table 1). We randomly selected 3 mutant (M1-M3) and 3 wild-type clones (W1-W3) from patient 1 and 3 mutant (m1-m3) and 3 wild-type clones (w1-w3) from patient 2 for the propagation and subsequent analyses.

All iPSC clones showed a characteristic human ESC-like morphology (Figure 1B), the reactivation of endogenous pluripotency genes (*OCT3/4*, *SOX2*, *NANOG*; Figure 1C-D; supplemental Figure 1D) and the demethylation of the *OCT3/4* promoter regions (supplemental Figure 1E). Transgene expression was rarely detected (Figure 1D; supplemental Figure 1D), and the retroviral integration patterns were confirmed by a Southern blot analysis (Figure 1E; supplemental Figure 1F). All of the iPSC clones maintained a normal karyotype (data not shown). There were neither proviral integration nor copy number changes observed in any of the genes that might affect the function of the NLRP3 inflammasome (supplemental Tables 1 and 2). Genetic identity was proven by a short tandem repeat analysis (supplemental Table 3), and the pluripotency of the iPSC clones was confirmed by the presence of cell derivatives of all 3 germ layers by teratoma formation after injection of undifferentiated iPSCs into immunocompromised NOD/scid/ $\gamma\text{c}^{\text{null}}$ mice (Figure 1F; supplemental Figure 1G).

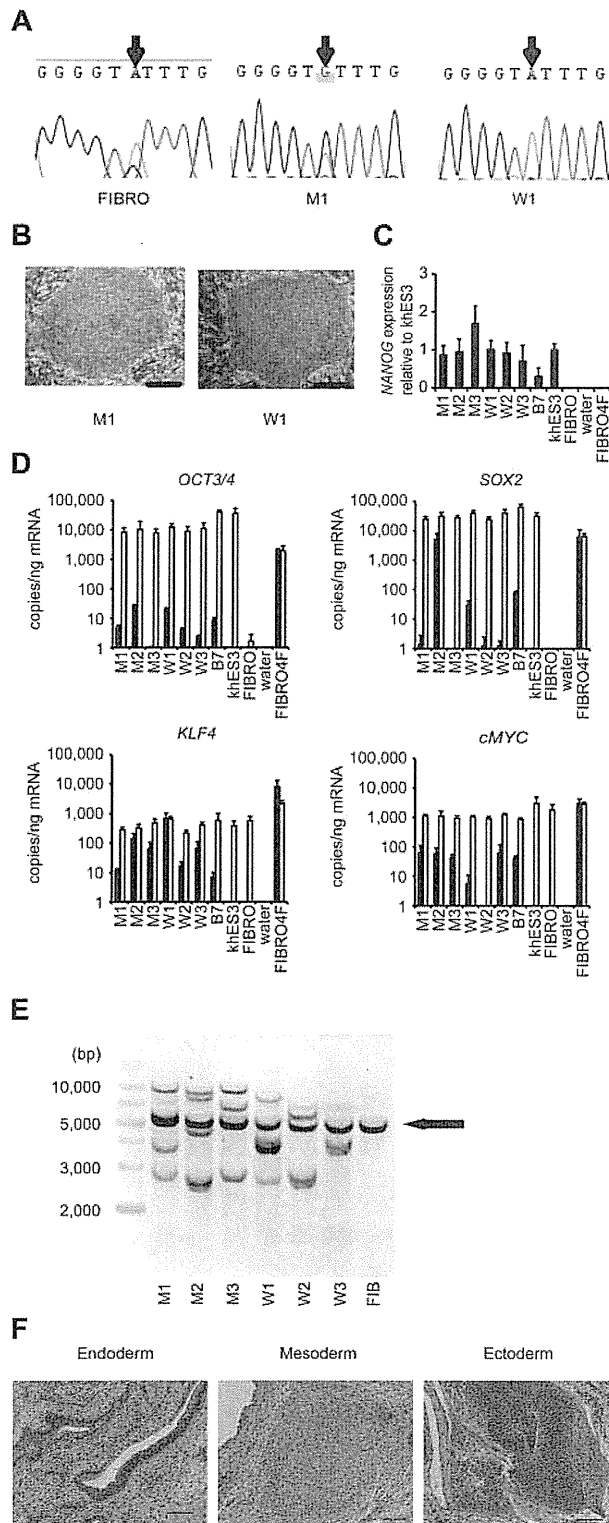


Figure 1. Establishment and characterization of iPSCs. (A) Sequencing of the *NLRP3* 1709 A > G mutation (Y570C) in fibroblasts (FIBRO), mutant iPSCs (M1), and wild-type iPSCs (W1) in patient 1. (B) The morphology of the mutant and wild-type iPSCs. (C) *NANOG* expression in CINCA iPSCs, control iPSCs (B7), control ESCs (khES3), fibroblasts (FIBRO), and fibroblasts transduced with 4 factors (FIBRO4F) normalized to *GAPDH*. $n = 3$. (D) A quantitative RT-PCR assay for the expression of *OCT3/4*, *SOX2*, *KLF4*, and *cMYC* in iPSCs. One primer set detects only the transgene (in black), and the other primer set detects both the transgene and endogenous gene (in white). $n = 3$. (E) Retroviral transgene integration analyses. Southern blot analyses were performed with DIG-labeled DNA probes against *c-MYC*. The parental fibroblasts carried a band in common with all of the iPSC lines (arrow). (F) A teratoma derived from a mutant iPSC clone, M1. Scale bars represent 100 μm . Data are mean \pm SEM.

Differentiation and characterization of iPSC-derived macrophages

To compare the most prominent features of the disease, we differentiated the patient-derived iPSCs into the monocyte/macrophage lineage using a murine stromal cell line, OP9.²¹ After culturing the iPSCs on an OP9 feeder layer for 10 days, we collected $\text{KDR}^+ \text{CD34}^+$ hemangioblasts (Figure 2A). All of the iPSC clones, whether they carried an *NLRP3* mutation or not, differentiated into $\text{KDR}^+ \text{CD34}^+$ progenitors as efficiently as the control ESC or iPSC clones (Figure 2B; supplemental Figure 2A). Adherent CD68^+ macrophages emerged after culturing the $\text{KDR}^+ \text{CD34}^+$ cells on another OP9 feeder layer for 16 days (Figure 2C; supplemental Figure 2B). Approximately 80% of the differentiated cells expressed CD14, and magnetic-activated cell sorting increased the purity to almost 100% (Figure 2D). All of the clones we used efficiently produced comparable amounts of iPSC-derived macrophages (iPS-MPs; Figure 2E; supplemental Figure 2C). The iPS-MPs visualized by light and electron microscopy showed a typical morphology, with a high cytoplasm-to-nucleus ratio and cytoplasmic vacuoles (Figure 2F; supplemental Figure 2D). The iPS-MPs showed a global gene expression pattern closer to that of blood-derived macrophages than to the parental iPSC clone (supplemental Figure 2E-F). Both mutant and wild-type iPS-MPs phagocytosed bacteria to the same extent when we infected the cells with Gram-positive LM, an intracellular bacterium that escapes into the cytosol (Figure 2G-H). These data indicate that both the mutant and wild-type iPS-MPs derived from mosaic CINCA patients are indistinguishable based on their gene expression and their phagocytic function.

Elucidation of the pathogenesis of somatic mosaic CINCA syndrome

Monocytes derived from CINCA syndrome patients usually do not spontaneously secrete IL-1 β and become active after LPS stimulation.⁶ Monocytes or mononuclear cells from untreated CINCA syndrome patients, however, sometimes show an increased synthesis of proIL-1 β ² and secretion of mature IL-1 β ,⁷ even in the absence of LPS stimulation, because they can be activated by persistent inflammation or by the purification procedure. As spontaneous activation complicates the functional analysis, we herein evaluated the IL-1 β activation status both before and after the stimulation. We observed that the mRNA expression of *IL1B* was low in unstimulated iPS-MPs and increased to comparable levels in mutant and wild-type iPS-MPs in response to LPS stimulation (supplemental Figure 3A). Similarly, the mRNA level of *NLRP3* was relatively low before LPS stimulation (supplemental Figure 3A). Mature IL-1 β was not detectable in the supernatant of the cell culture medium (data not shown). Collectively, these data indicate that the unstimulated iPS-MPs were in an “inactive” state before stimulation.

To identify which iPS-MP clones showed the specific features compatible to patients’ monocytes, we evaluated their IL-1 β secretion. Although LPS stimulation alone led to IL-1 β secretion

Table 1. Mutation frequency among different cell types

Patient no.	Site of mutation	Frequency (%) of mutant cells		
		Whole blood*	Fibroblasts	iPSCs
1	1709A > G(Y570C)	33.3	34.3	42.9
2	919G > A(G307S)	8.5	9.8	10.0

*The frequency in whole blood was reported previously.^{9,20}

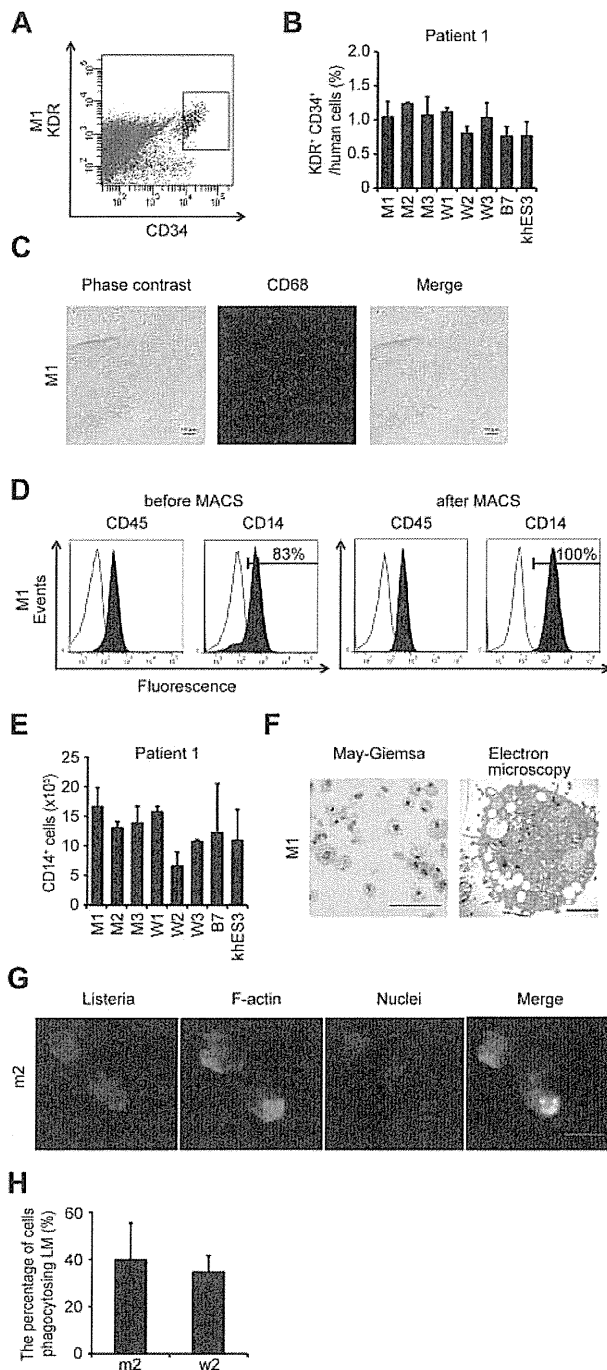


Figure 2. Differentiation and characterization of iPSCs-derived macrophages. (A) KDR⁺ CD34⁺ hematopoietic progenitors purified 10 days after differentiation. (B) The percentage of KDR⁺ CD34⁺ cells in Tra-1-85⁺ human cells. $n = 3$. (C) CD68 immunostaining of macrophages. Scale bars represent 100 μm . (D) The histograms show antibody staining (in black) relative to the isotype-matched controls (in white) for a blood cell marker (CD45), and a macrophage marker (CD14), in cells before (left 2 panels) or after (right 2 panels) magnetic-activated cell sorting purification. (E) CD14⁺ cell counts obtained from iPSCs plated on an OP9 feeder layer on one 100-mm dish. $n = 3$. (F) Representative morphology of iPSC-MPs evaluated by May-Giemsa staining or transmission electron microscopy. Scale bars represent 100 μm and 2 μm , respectively. (G) The phagocytosis by iPSC-MPs after LM infection. The cells were treated with anti-LM antibody, phalloidin, and 4',6'-diamidino-2-phenylindole. Scale bar represents 20 μm . (H) The percentage of iPSC-MPs phagocytosing LM was calculated as the average of 9 fields of vision. Data are mean \pm SEM.

from the mutant iPSC-MPs, the addition of ATP was necessary to induce IL-1 β secretion from wild-type iPSC-MPs, as it was from either ESC-derived or blood-derived macrophages (Figure 3A).

The IL-1 β level from mutant iPSC-MPs was significantly higher than that from wild-type macrophages, even in the presence of LPS plus ATP. Both groups of macrophages showed similar kinetics in their secretion of other cytokines, such as IL-6 or TNF α (Figure 3A). The results were similar in the iPSC-MPs from patient 2 (Figure 3B). Although iPSC-MPs showed a similar response at lower LPS concentrations (Figure 3C-D; supplemental Figure 3B-C), no IL-1 β secretion was detectable from mutant iPSCs, wild-type iPSCs, or parental fibroblasts in response to stimulation with 1 $\mu\text{g}/\text{mL}$ LPS (data not shown). These data demonstrate that the abnormal function of the iPSC-MPs is predominantly determined by the *NLRP3* mutation, and not by some unknown genetic alteration(s) prevalent in all cells. We next investigated whether iPSC-MPs show pyronecrosis: a pathogen-induced, cathepsin B-dependent, necrosis-like programmed cell death that is characteristically observed in *NLRP3*-mutant monocytes/macrophages.^{22,23} When we compared LDH secretion as a marker of membrane rupture, we found that LPS stimulation evoked a significantly higher LDH secretion only from the mutant iPSC-MPs, which was inhibited by the cathepsin B inhibitor, CA074Me (Figure 3E).

Despite the low percentage of mutant cells, the clinical manifestation of mosaic CINCA patients is similar to that of patients with a heterozygous mutation.^{9,10} We hypothesized that an interaction between the mutant and wild-type macrophages leads to exacerbation of the inflammation. To test this hypothesis, we modeled a mosaic condition by coculturing mutant and wild-type cells. After stimulating mutant iPSC-MPs with LPS in separate cultures or in cocultures with wild-type counterparts, we determined the IL-1 β level in the supernatant. We found that the IL-1 β secretion significantly increased after coculture (Figure 4A; supplemental Figure 4A). Although increasing the cell concentration raised the total amount of the IL-1 β secretion from mutants, it did not accelerate the IL-1 β secretion per cell from mutant iPSC-MPs or enhance the secretion from wild-type macrophages (Figure 4B). To determine the ratio of mutant/wild-type cells at which the additional IL-1 β secretion is most enhanced, we changed the ratio using a fixed number of mutant iPSC-MPs and increasing the number of wild-type iPSC-MPs. We observed a significant increase only at a percentage of 25% mutant macrophages (Figure 4C). Thus, we recapitulated, at least in part, the patient's mosaic condition in vitro.

Next, we tried to elucidate whether the interaction is mediated by some humoral factor(s), but supernatant transfer did not facilitate the IL-1 β secretion (Figure 4D). As a candidate that may mediate this interaction, we selected ATP because necrotic cells trigger *NLRP3*-inflammasome activation in part through ATP release.²⁴ We therefore investigated whether the necrosis-induced ATP secretion activates the wild-type iPSC-MPs using ATP receptor antagonists, oxidized ATP (oATP) and PPADS. Although both antagonists markedly inhibited the IL-1 β secretion after LPS plus ATP stimulation (supplemental Figure 4B), neither of them abrogated the additional IL-1 β secretion in the mixed culture (Figure 4E; compare column 2 with column 3, and column 4 with column 5). The IL-1 β secretion from mutant iPSC-MPs may have decreased because of off-target effects of oATP.²⁵ Overall, although it remains to be elucidated how this effect is mediated, these results suggest that the interaction between mutant and wild-type macrophages may enhance IL-1 β secretion in mosaic patients.

Validation for future applications for drug screening

An *NLRP3*-targeted therapeutic approach would be attractive because (1) the progressive arthropathy despite anti-IL-1 therapy indicates that the presence of additional proteins processed by the

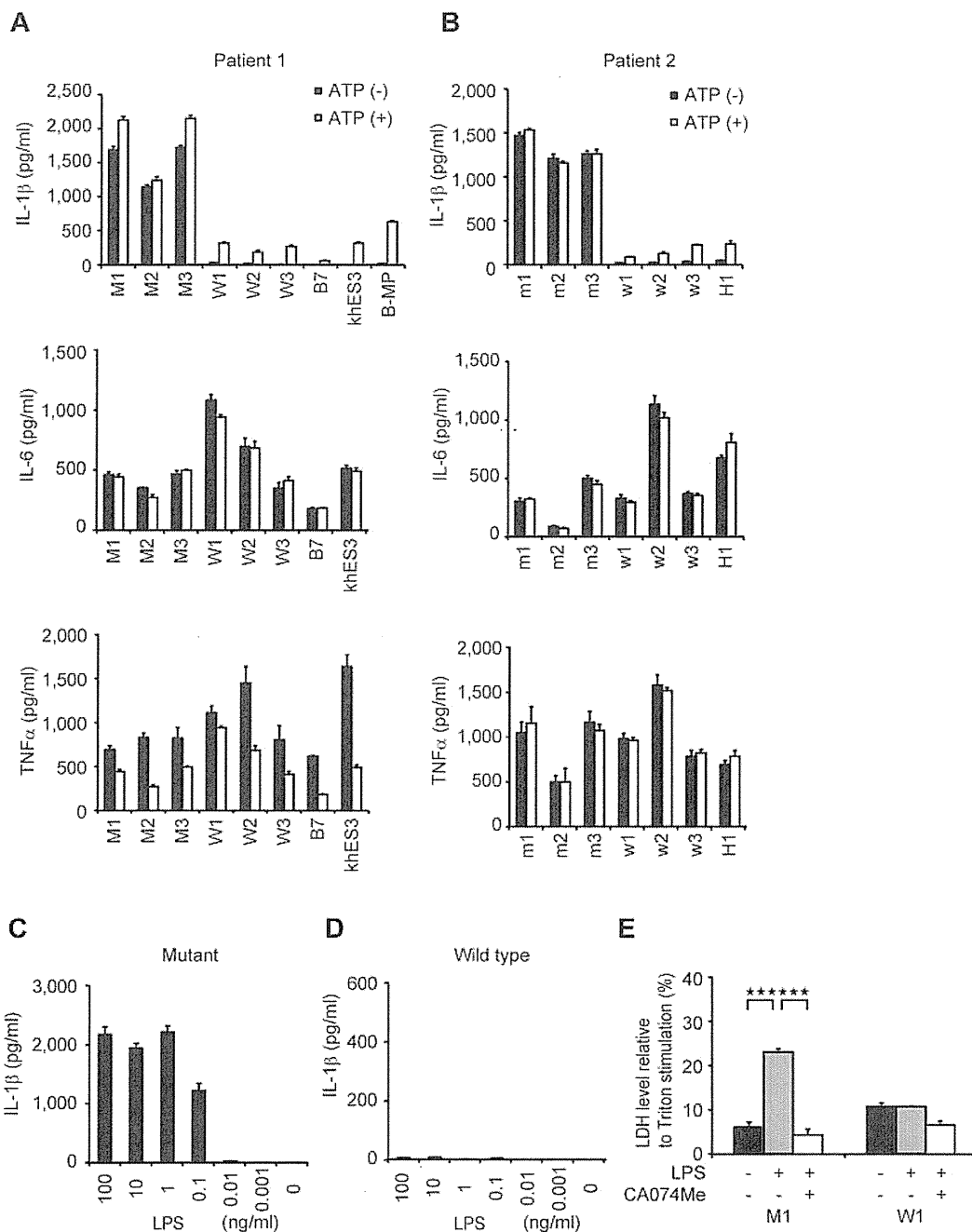


Figure 3. Elucidation of the pathogenesis of somatic mosaic CINCA syndrome. (A) Cytokine secretion from iPS-MPs derived from patient 1. After stimulating iPS-MPs by LPS with or without ATP, we determined the IL-1 β (top panel), IL-6 (middle panel), or TNF α (bottom panel) level of the supernatant. $n = 3$. (B) Cytokine secretion from iPS-MPs derived from patient 2, determined as in panel A. (C) IL-1 β secretion from mutant iPS-MPs in the presence of 10-fold dilutions of LPS from 100 ng/mL. $n = 3$. (D) IL-1 β secretion from wild-type iPS-MPs, determined as in panel C. (E) LDH secretion from iPS-MPs stimulated with LPS in the presence or absence of the cathepsin B inhibitor, CA074Me. $n = 3$. Data are mean \pm SEM. *** $P < .001$ (Student t test).

inflammasome is also involved in the pathogenesis of CINCA syndrome; (2) specific inhibition of the NLRP3-inflammasome can avoid unfavorable suppression of other IL-1 β -processing pathways in response to various triggers; and (3) these drugs may be also effective for various other NLRP3-related chronic inflammatory conditions, such as Alzheimer disease, diabetes, severe gout, and atherosclerosis.²⁶⁻³⁰ Because drug screening using NLRP3 autoactivated cells has not been described previously, we examined whether the iPS-MPs from CINCA patients can serve as a prototype for seeking drug candidates that directly modulate NLRP3-inflammasome activation.

When wild-type iPS-MPs were stimulated with LPS and ATP in the presence of various inhibitors, inhibitors known to modulate molecules upstream of the NLRP3-inflammasome (a protein synthesis inhibitor, cycloheximide, and an NF- κ B inhibitor, MG132), downstream of the inflammasome (a caspase-1 inhibitor, Ac-YVAD-CHO), and both upstream of and the inflammasome itself³¹ (Bay11-7082) successfully inhibited IL-1 β secretion (Figure 5A). Although the precise mechanism is unknown, a cathepsin B inhibitor, CA074Me, also efficiently inhibited IL-1 β secretion. As expected, upstream inhibitors inhibited the secretion of other cytokines, such as IL-6 and IL-8, but a downstream inhibitor,

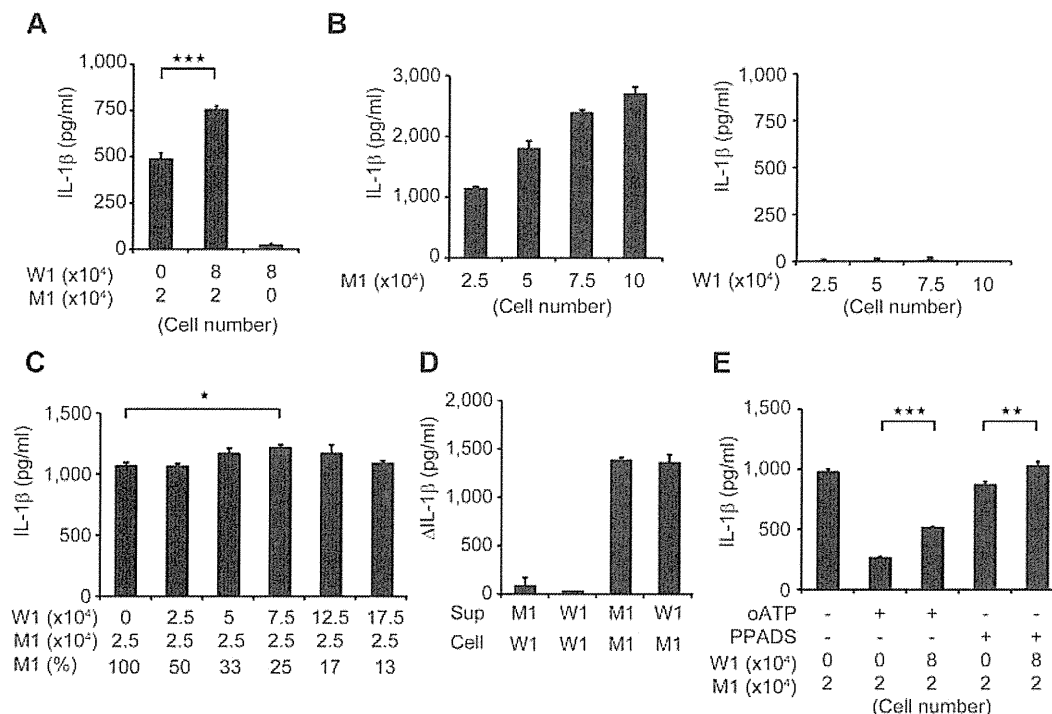


Figure 4. Remodeling mosaicism by coculturing mutant and wild-type iPSC-MPs. (A) IL-1 β secretion from cocultured iPSC-MPs. We used 2×10^4 mutant iPSC-MPs (M1) and 8×10^4 wild-type iPSC-MPs (W1) as indicated. $n = 6$. (B) IL-1 β secretion from various numbers of mutant (left panel) or wild-type (right panel) iPSC-MPs. The iPSC-MPs were seeded at the indicated numbers. $n = 3$. (C) IL-1 β secretion from iPSC-MPs that were cocultured at various ratios. The wild-type or mutant iPSC-MPs were seeded at the numbers indicated in the first and second rows, respectively. The percentage of mutants is indicated in the third row; $n = 3$. (D) Increase of IL-1 β levels during stimulation by the supernatant. The supernatant was harvested from the wells of the indicated iPSC-MPs (Sup) and transferred to the wells of other iPSC-MPs (Cell); $n = 3$. (E) IL-1 β secretion from cocultured iPSC-MPs in the presence of the ATP receptor antagonist, α ATP (300 μ M) or PPADS (300 μ M). We used 2×10^4 mutant iPSC-MPs (M1) and 8×10^4 wild-type iPSC-MPs (W1) as indicated. $n = 6$. Data are mean \pm SEM. *** $P < .001$ (Student *t* test). ** $P < .01$ (Student *t* test). * $P < .05$ (Student *t* test).

Ac-YVAD-CHO, specifically affected IL-1 β secretion (Figure 5A). Although CA074Me and Ac-YVAD-CHO inhibited IL-1 β secretion regardless of the second signals that were present, PPADS, an inhibitor of extracellular ATP signaling, failed to inhibit IL-1 β secretion by following exposure to other second signals, such as monosodium urate and silica crystals (Figure 5B), proving that wild-type iPSC-MPs can be activated in a second signal-dependent manner. Therefore, the results of the wild-type iPSC-MP-based compound screening depended on the choice of second signals, and such a screening makes it possible to extract candidate compounds that modulate specific second signaling pathways.

Next, we examined the response of mutant iPSC-MPs to the inhibitors. In the absence of inhibitors, mutant iPSC-MPs secreted a higher level of IL-1 β , but treatment with inhibitors dose-dependently decreased IL-1 β secretion to the comparable level produced by WT iPSC-MPs (Figure 5C). We thus demonstrated the efficacy of these chemical compounds, even for excessive IL-1 β production by constitutively hyperactivated inflammasomes. As expected, the mutant iPSC-MPs did not respond to PPADS, confirming their autoactivation in a second signal-independent manner (Figure 5D). Therefore, because they can be activated independently from the type of second signals, mutant iPSC-MP-based screening would enable the exclusion of compounds that inhibit IL-1 β secretion depending on a specific type of second signal transduction. Overall, through using the IL-1 β inhibition as the initial criteria and weeding out upstream inhibitors by measuring the levels of other cytokines, we can use *NLRP3*-mutant iPSC-MPs to screen for drugs for CINCA syndrome and possibly for other *NLRP3*-related chronic inflammatory conditions.

Discussion

Since the first identification of a CINCA syndrome patient carrying *NLRP3* mutation as somatic mosaicism,²⁰ it has been controversial whether the small fraction of *NLRP3*-mutated cells actually causes the strong autoinflammation. It remained unanswered because of the difficulty to separately obtain live mutant and nonmutant blood cells. In this study, we reprogrammed fibroblasts from mosaic patients and obtained macrophages with different genotypes. By showing that only *NLRP3*-mutant iPSC-MPs exhibit the distinct proinflammatory phenotype, we demonstrated that the *NLRP3*-mutant macrophages are mainly responsible for the pathogenesis of mosaic CINCA syndrome.

In this study, we established both *NLRP3*-mutant and nonmutant iPSC clones from the same person. One of the potential limitations of studies with patient-derived iPSCs is the difficulty in obtaining isogenic control counterparts, which do not carry the responsible mutations. One possible strategy to solve this problem is to correct the affected gene locus of patient-derived iPSC clones using novel techniques that facilitate homologous recombination.^{32,33} As another solution, both affected and control iPSC clones can be obtained from patients of some X-linked hereditary diseases because each iPSC clone originated from somatic cells carrying either a mutated or nonmutated allele as an active X chromosome.³⁴⁻³⁶ In the present study, we have retrieved both mutant and wild-type iPSC clones from patients with somatic autosomal mutations. These clones theoretically have the same genetic backgrounds, except for the *NLRP3* gene, and should serve as an ideal pair of mutant and control clones for disease research.

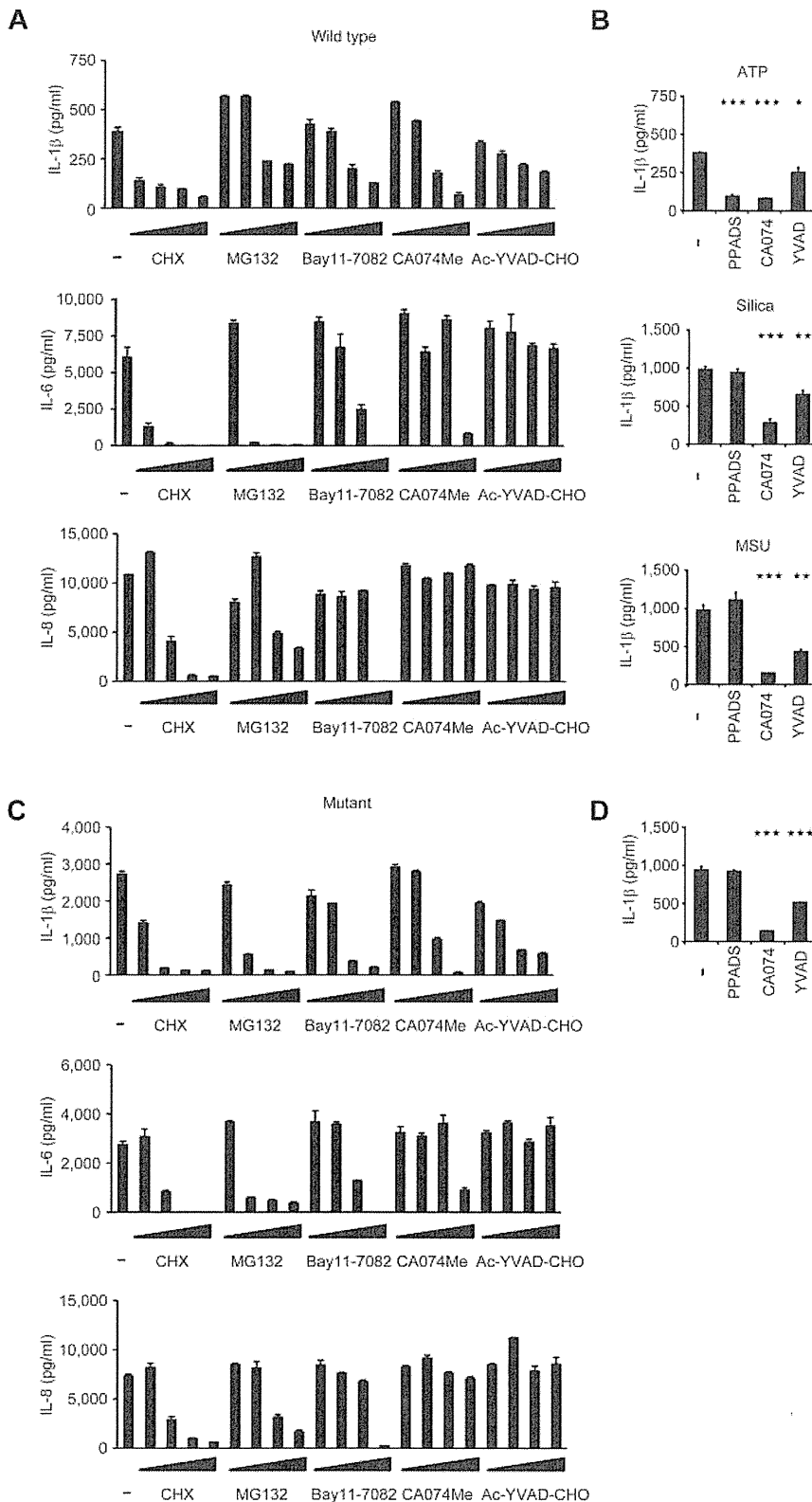


Figure 5. Validation of the cells for future applications for drug screening. (A) Inhibition of IL-1 β (top panel), IL-6 (middle panel), or IL-8 (bottom panel) secretion from wild-type iPS-MPs by various inhibitors. The iPS-MPs were cultured for 2 hours in the presence of 100 μ M cycloheximide (CHX), 100 μ M MG132, 10 μ M Bay11-7082, 25 μ M CA074Me, 50 μ M Ac-YVAD-CHO, as well as 10-fold dilutions of each inhibitor, except CA074Me (which was diluted 5-fold), followed by LPS treatment plus ATP stimulation. $n = 3$. (B) The differential inhibition of IL-1 β secretion from wild-type iPS-MPs by various inhibitors. In the presence of inhibitors, such as PPADS (300 μ M), CA074Me (25 μ M), or Ac-YVAD-CHO (50 μ M), LPS-primed wild-type iPS-MPs were stimulated with second signal triggers, such as ATP for 1 hour (top panel), silica crystals for 1 hour (middle panel), or monosodium urate crystals for 3 hours (bottom panel). $n = 3$. (C) Inhibition of IL-1 β (top panel), IL-6 (middle panel), or IL-8 (bottom panel) secretion from mutant iPS-MPs by various inhibitors was evaluated as in panel A; $n = 3$. (D) Inhibition of IL-1 β secretion from mutant iPS-MPs by various inhibitors. In the presence of inhibitors, such as PPADS (300 μ M), CA074Me (25 μ M), or Ac-YVAD-CHO (50 μ M), mutant iPS-MPs were stimulated with LPS for 4 hours. $n = 3$. Data are mean \pm SEM. *** $P < .001$ (Student t test). ** $P < .01$ (Student t test). * $P < .05$ (Student t test).

In addition to obtaining isogenic controls, iPSCs from patients with somatic autosomal mutations enable dissection and modeling of somatic mosaicism. Despite the fact that each person contains various minor somatic mutations,³⁷ the effects of mosaicism can often be overlooked because of the difficulty in assessing the possible biologic effects caused by the small cell populations carrying the genetic alterations. Here we dissected somatic mosa-

icism by obtaining the component cells with heterogeneous genetic identity separately and established an in vitro model to evaluate the interaction between these cells, although precise mechanism of interaction remains to be elucidated. As an approach to determining the disease-causing potential of a specific somatic mutation found in a person, iPSC technology provides advantages compared with ordinary methods, such as the use of transgenic cell lines. First,

iPSCs can be differentiated into the affected cell types or tissues, allowing direct functional assays to be performed that are associated with the pathology. Second, because the disease-causing potential of some mutations is dependent on the genetic backgrounds of the patients,³⁸ it may be better to obtain both mutant and wild-type clones from a single mosaic patient to more accurately assess the impact of the mutation(s).

Considering that a mutation of *NLRP3* in 10% of the cells is sufficient to cause a distinct disease phenotype, somatic mutations of various genes at an even rarer frequency may also affect the biologic characteristics of a person. Because the presence of the *NLRP3* mutation did not affect the efficacy of reprogramming to the iPSCs, we may be able to obtain both mutant and wild-type iPSC clones from CINCA syndrome patients who carry *NLRP3* mutant cells at a lower percentage. In some diseases, such as Fanconi anemia, however, mutant cells may be resistant to reprogramming.^{39,40} Even though there are some possible limitations, establishing both mutant and wild-type iPSC clones is a promising approach to dissect the extent and role of somatic mosaicism.

We demonstrated that several inhibitors that are considered to be effective against CINCA syndrome actually attenuated the disease-relevant phenotype of iPSC-derived macrophages. Before a successful drug screening using iPSC-derived somatic cells can be developed, several limitations need to be overcome, such as the heterogeneity of differentiation and difficulties associated with purification.¹⁸ In this report, we used an efficient and robust differentiation protocol and obtained plenty of macrophages free from the clonal variations.

In conclusion, we elucidated the pathologic roles of both mutant and wild-type cells in mosaic CINCA syndrome patients. After obtaining iPSC-derived macrophages in large quantity and with high purity, we showed they are applicable for drug screening. The iPSC-based approach may help to illuminate the pathogenesis of various diseases that are caused by somatic mosaicism, and facilitate drug discovery for the treatment of *NLRP3*-related inflammatory diseases.

Acknowledgments

The authors thank the CINCA syndrome patients who participated in this study; Y. Sasaki, Y. Jindai, A. Okada, M. Narita,

A. Nagahashi, T. Ohkame, S. Nishimoto, Y. Inoue, and S. Arai for technical assistance; I. Kato for help with animal experiments; M. Nakagawa, K. Okita, Y. Yoshida, T. Aoi, and M. Yanagimachi for scientific comments; and R. Kato, E. Nishikawa, S. Takeshima, Y. Otsu, H. Hasaba, H. Watanabe, T. Ishii, H. Kurokawa, N. Takasu, and Y. Takao for administrative assistance.

This work was supported by the Ministry of Health, Labor and Welfare (N.M. and T.N.), the Ministry of Education, Culture, Sports, Science and Technology (MEXT; N.M. and T.N.), the Leading Project of MEXT (S.Y. and T.N.), the Promotion of Fundamental Studies in Health Sciences of National Institute of Biomedical Innovation (S.Y.), the Funding Program for World-Leading Innovative Research and Development on Science and Technology (FIRST Program) of Japan Society for the Promotion of Science (JSPS; T.N., and S.Y.), JSPS and MEXT (Grants-in-Aid for Scientific Research; S.Y.), JSPS (T.N., T.T., and M.K.S.), the Takeda Science Foundation, SENSHIN Medical Research Foundation, and Suzuken Memorial Foundation to (M.K.S.).

Authorship

Contribution: T.T. planned the project, established iPSCs, performed experimental work, analyzed data, and prepared the manuscript; K.T. planned the project, established iPSCs, and analyzed data; M.Y., S.T., and S.N. performed experimental work; K.O., A.N., and T.H. analyzed data; R.N. and N.K. planned the project; H.H. and M.M. performed *L monocytogenes* infection; N.M. and J.E.H. performed electron microscopy; T.Y. identified retroviral integration sites; A.W. performed bisulfite sequencing; A.S.-O. and S.O. analyzed CNV; I.A. established iPSCs; S.Y. and T.N. planned the project and analyzed data; M.K.S. planned the project, analyzed data, and prepared the manuscript; and all authors read and approved the manuscript.

Conflict-of-interest disclosure: S.Y. is a member without salary of the scientific advisory boards of iPierian, iPS Academia Japan, and Megakaryon Corporation. The remaining authors declare no competing financial interests.

Correspondence: Megumu K. Saito, Center for iPS Cell Research and Application, Kyoto University, Kyoto 606-8507, Japan; e-mail: msaito@cira.kyoto-u.ac.jp.

References

- Prieur AM, Griscelli C, Lampert F, et al. A chronic, infantile, neurological, cutaneous and articular (CINCA) syndrome: a specific entity analysed in 30 patients. *Scand J Rheumatol Suppl.* 1987;66:57-68.
- Aksentijevich I, Nowak M, Mallah M, et al. De novo CIAS1 mutations, cytokine activation, and evidence for genetic heterogeneity in patients with neonatal-onset multisystem inflammatory disease (NOMID): a new member of the expanding family of pyrin-associated autoinflammatory diseases. *Arthritis Rheum.* 2002;46(12):3340-3348.
- Feldmann J, Prieur AM, Quartier P, et al. Chronic infantile neurological cutaneous and articular syndrome is caused by mutations in CIAS1, a gene highly expressed in polymorphonuclear cells and chondrocytes. *Am J Hum Genet.* 2002;71(1):198-203.
- Bauernfeind FG, Horvath G, Stutz A, et al. Cutting edge: NF- κ B activating pattern recognition and cytokine receptors license *NLRP3* inflammasome activation by regulating *NLRP3* expression. *J Immunol.* 2009;183(2):787-791.
- Mariathasan S, Weiss DS, Newton K, et al. Cryopyrin activates the inflammasome in response to toxins and ATP. *Nature.* 2006;440(7081):228-232.
- Gattorno M, Tassi S, Carta S, et al. Pattern of interleukin-1 β secretion in response to lipopolysaccharide and ATP before and after interleukin-1 blockade in patients with CIAS1 mutations. *Arthritis Rheum.* 2007;56(9):3138-3148.
- Goldbach-Mansky R, Dailey NJ, Canna SW, et al. Neonatal-onset multisystem inflammatory disease responsive to interleukin-1 β inhibition. *N Engl J Med.* 2006;355(6):581-592.
- Neven B, Marvillet I, Terrada C, et al. Long-term efficacy of the interleukin-1 receptor antagonist anakinra in ten patients with neonatal-onset multisystem inflammatory disease/chronic infantile neurologic, cutaneous, articular syndrome. *Arthritis Rheum.* 2010;62(1):258-267.
- Saito M, Nishikomori R, Kambe N, et al. Disease-associated CIAS1 mutations induce monocyte death, revealing low-level mosaicism in mutation-negative cryopyrin-associated periodic syndrome patients. *Blood.* 2008;111(4):2132-2141.
- Tanaka N, Izawa K, Saito MK, et al. High incidence of *NLRP3* somatic mosaicism in patients with chronic infantile neurologic, cutaneous, articular syndrome: results of an International Multi-center Collaborative Study. *Arthritis Rheum.* 2011;63(11):3625-3632.
- Masters SL, Simon A, Aksentijevich I, Kastner DL. Horror autoinflammatory: the molecular pathophysiology of autoinflammatory disease. *Annu Rev Immunol.* 2009;27:621-668.
- Youssoufian H, Pyeritz RE. Mechanisms and consequences of somatic mosaicism in humans. *Nat Rev Genet.* 2002;3(10):748-758.
- Erickson RP. Somatic gene mutation and human disease other than cancer: an update. *Mutat Res.* 2010;705(2):96-106.
- Ariga T, Kondoh T, Yamaguchi K, et al. Spontaneous in vivo reversion of an inherited mutation in the Wiskott-Aldrich syndrome. *J Immunol.* 2001;166(8):5245-5249.

15. Nishikomori R, Akutagawa H, Maruyama K, et al. X-linked ectodermal dysplasia and immunodeficiency caused by reversion mosaicism of NEMO reveals a critical role for NEMO in human T-cell development and/or survival. *Blood*. 2004; 103(12):4565-4572.
16. Lutskiy MI, Beardsley DS, Rosen FS, Remold-O'Donnell E. Mosaicism of NK cells in a patient with Wiskott-Aldrich syndrome. *Blood*. 2005;106(8):2815-2817.
17. Takahashi K, Tanabe K, Ohnuki M, et al. Induction of pluripotent stem cells from adult human fibroblasts by defined factors. *Cell*. 2007;131(5):861-872.
18. Grskovic M, Javaherian A, Strulovici B, Daley GQ. Induced pluripotent stem cells: opportunities for disease modelling and drug discovery. *Nat Rev Drug Discov*. 2011;10(12):915-929.
19. Hanna J, Markoulaki S, Schorderet P, et al. Direct reprogramming of terminally differentiated mature B lymphocytes to pluripotency. *Cell*. 2008;133(2):250-264.
20. Saito M, Fujisawa A, Nishikomori R, et al. Somatic mosaicism of CIAS1 in a patient with chronic infantile neurologic, cutaneous, articular syndrome. *Arthritis Rheum*. 2005;52(11):3579-3585.
21. Nakano T, Kodama H, Honjo T. Generation of lymphohematopoietic cells from embryonic stem cells in culture. *Science*. 1994;265(5175):1098-1101.
22. Fujisawa A, Kambe N, Saito M, et al. Disease-associated mutations in CIAS1 induce cathepsin B-dependent rapid cell death of human THP-1 monocytic cells. *Blood*. 2007;109(7):2903-2911.
23. Willingham SB, Bergstraal DT, O'Connor W, et al. Microbial pathogen-induced necrotic cell death mediated by the inflammasome components CIAS1/cryopyrin/NLRP3 and ASC. *Cell Host Microbe*. 2007;2(3):147-159.
24. Iyer SS, Pulskens WP, Sadler JJ, et al. Necrotic cells trigger a sterile inflammatory response through the Nlrp3 inflammasome. *Proc Natl Acad Sci U S A*. 2009;106(48):20388-20393.
25. Beigi RD, Kertesz SB, Aquilina G, Dubyak GR. Oxidized ATP (oATP) attenuates proinflammatory signaling via P2 receptor-independent mechanisms. *Br J Pharmacol*. 2003;140(3):507-519.
26. Martinon F, Petrilli V, Mayor A, Tardivel A, Tschopp J. Gout-associated uric acid crystals activate the NALP3 inflammasome. *Nature*. 2006; 440(7081):237-241.
27. Halle A, Hornung V, Petzold GC, et al. The NALP3 inflammasome is involved in the innate immune response to amyloid-beta. *Nat Immunol*. 2008;9(8):857-865.
28. Duestell P, Kono H, Rayner KJ, et al. NLRP3 inflammasomes are required for atherogenesis and activated by cholesterol crystals. *Nature*. 2010; 464(7293):1357-1361.
29. Masters SL, Dunne A, Subramanian SL, et al. Activation of the NLRP3 inflammasome by islet amyloid polypeptide provides a mechanism for enhanced IL-1beta in type 2 diabetes. *Nat Immunol*. 2010;11(10):897-904.
30. Vandanmagsar B, Youm YH, Ravussin A, et al. The NLRP3 inflammasome instigates obesity-induced inflammation and insulin resistance. *Nat Med*. 2011;17(2):179-188.
31. Juliana C, Fernandes-Alnemri T, Wu J, et al. Anti-inflammatory compounds parthenolide and Bay 11-7082 are direct inhibitors of the inflammasome. *J Biol Chem*. 2010;285(13):9792-9802.
32. Aizawa E, Hirabayashi Y, Iwanaga Y, et al. Efficient and accurate homologous recombination in hESCs and hiPSCs using helper-dependent adenoviral vectors. *Mol Ther*. 2012;20(2):424-431.
33. Soldner F, Laganieri J, Cheng AW, et al. Generation of isogenic pluripotent stem cells differing exclusively at two early onset Parkinson point mutations. *Cell*. 2011;146(2):318-331.
34. Cheung AY, Horvath LM, Grafodatskaya D, et al. Isolation of MECP2-null Rett syndrome patient hiPS cells and isogenic controls through X-chromosome inactivation. *Hum Mol Genet*. 2011;20(11):2103-2115.
35. Kim KY, Hysolli E, Park IH. Neuronal maturation defect in induced pluripotent stem cells from patients with Rett syndrome. *Proc Natl Acad Sci U S A*. 2011;108(34):14169-14174.
36. Pomp O, Dreesen O, Leong DF, et al. Unexpected X chromosome skewing during culture and reprogramming of human somatic cells can be alleviated by exogenous telomerase. *Cell Stem Cell*. 2011;9(2):156-165.
37. Gore A, Li Z, Fung HL, et al. Somatic coding mutations in human induced pluripotent stem cells. *Nature*. 2011;471(7336):63-67.
38. Crotti L, Lundquist AL, Insolia R, et al. KCNH2-K897T is a genetic modifier of latent congenital long-QT syndrome. *Circulation*. 2005;112(9):1251-1258.
39. Raya A, Rodriguez-Piza I, Guenechea G, et al. Disease-corrected haematopoietic progenitors from Fanconi anemia induced pluripotent stem cells. *Nature*. 2009;460(7251):53-59.
40. Müller LU, Milsom MD, Harris CE, et al. Overcoming reprogramming resistance of Fanconi anemia cells. *Blood*. 2012;119(23):5449-5457.

LETTERS TO THE EDITOR

Novel splicing-factor mutations in juvenile myelomonocytic leukemia

Leukemia (2012) 26, 1879–1881; doi:10.1038/leu.2012.45

Myelodysplastic syndromes (MDS) and myelodysplastic/myeloproliferative neoplasms (MDS/MPN) are heterogeneous groups of chronic myeloid neoplasms characterized by clonal hematopoiesis, varying degrees of cytopenia or myeloproliferative features with evidence of myelodysplasia and a propensity to acute myeloid leukemia (AML).¹ In recent years, a number of novel gene mutations, involving *TET2*, *ASXL1*, *DNMT3A*, *EZH2*, *IDH1/2*, and *c-CBL*, have been identified in adult cases of chronic myeloid neoplasms, which have contributed to our understanding of disease pathogenesis.^{2–7} However, these mutations are rare in pediatric cases, with the exception of germline or somatic *c-CBL* mutations found in 10–15% of chronic myelomonocytic leukemia (CMML) and juvenile myelomonocytic leukemia (JMML),⁸ highlighting the distinct pathogenesis of adult and pediatric neoplasms.⁹

Recently, we reported high frequencies of mutations, involving the RNA splicing machinery, that are largely specific to myeloid neoplasms, showing evidence of myeloid dysplasia in adult.¹⁰ Affecting a total of eight components of the RNA splicing machinery (*U2AF35*, *U2AF65*, *SF3A1*, *SF3B1*, *SRSF2*, *ZRSR2*, *SF1* and *PRPF40B*) commonly involved in the 3' splice-site (3'SS) recognition, these pathway mutations are now implicated in the pathogenesis of myelodysplasia.¹⁰ To investigate the role of the splicing-pathway mutations in the pathogenesis of pediatric myeloid malignancies, we have examined 165 pediatric cases with AML, MDS, chronic myeloid leukemia (CML) and JMML for

mutations in the four major splicing factors, *U2AF35*, *ZRSR2*, *SRSF2*, and *SF3B1*, commonly mutated in adult cases.

Bone marrow or peripheral blood tumor specimens were obtained from 165 pediatric patients with various myeloid malignancies, including *de novo* AML ($n=93$), MDS ($n=28$), CML ($n=17$) and JMML ($n=27$), and the genomic DNA (gDNA) was subjected to mutation analysis (Supplementary Table 1). The status of the RAS pathway mutations for the current JMML series has been reported previously (Supplementary Table 2).^{11,12} Nineteen leukemia cell lines derived from AML (YNH-1, ML-1, KASUMI-3, KG-1, HL60, inv-3, SN-1, NB4 and HEL), acute monocytic leukemia (THP-1, SCC-3, J-111, CTS, P31/FUJ, MOLM-13, IMS/MI and KOCL-48) and acute megakaryoblastic leukemia (CMS and CMY) were also analyzed for mutations. Peripheral blood gDNA from 60 healthy adult volunteers was used as controls. Informed consent was obtained from the patients and/or their parents and from the healthy volunteers. We previously showed that for *U2AF35*, *SRSF2* and *SF3B1*, most of the mutations in adult cases were observed in exons 2 and 7, exon 1, and exons 14 and 15, respectively.¹⁰ Therefore, we confirmed mutation screening to these 'hot-spot' exons. In contrast, all the coding exons were examined for *ZRSR2*, because no mutational hot spots have been detected. Briefly, the relevant exons were amplified using PCR and mutations were examined by Sanger sequencing, as previously described.¹⁰ The Fisher's exact test was used to evaluate the statistical significance of frequencies of mutations for *U2AF35*, *SF3B1*, *ZRSR2* or *SRSF2* in adult cases and pediatric cases. This study was approved by the Ethics Committee of the University of Tokyo (Approval number 948-7).

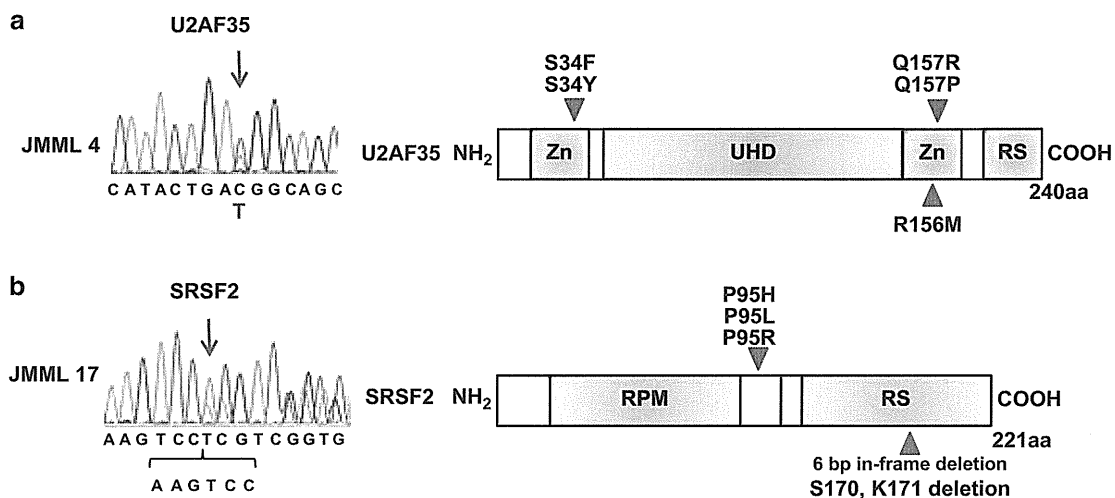


Figure 1. Novel *U2AF35* and *SRSF2* mutations detected in JMML cases. (a) Left panel: sequence chromatogram of a heterozygous mutation at R156 in N-terminal zinc-finger motifs of *U2AF35* detected in a JMML case (JMML 4) is shown. Mutated nucleotides are indicated by arrows. Right panel: illustration of functional domains and mutations of *U2AF35*. Red arrow heads indicate hot-spot mutations at S34 and Q157 detected in the adult cases.¹⁰ Blue arrow head indicates the missense mutation at R156. (b) Left panel: sequence chromatogram of a 6-bp in-frame deletion (c.518-523delAAGTCC) in *SRSF2* detected in JMML 17 is shown. Mutated nucleotides are indicated by arrows. Right panel: illustration of functional domains and mutations of *SRSF2*. Red arrow head indicates hot-spot mutation at P95 frequently detected in the adult cases.¹⁰ Blue arrow head indicates a 6-bp in-frame deletion leading to deletion of S170 and K171.

No mutations were identified in the 28 cases with pediatric MDS, which included 13 cases with refractory anemia with excess blasts, 5 with refractory cytopenia of childhood, 2 with Down syndrome-related MDS, 2 with Fanconi anemia-related MDS, 2 with secondary MDS and 4 with unclassified MDS. Similarly, no mutations were detected in 93 cases with *de novo* AML or in 17 with CML, as well as 19 leukemia-derived cell lines. Our previous study in adult patients showed the frequency of mutations in *U2AF35*, *SF3B1*, *ZRSR2* or *SRSF2* to be 60/155 cases with MDS without increased ring sideroblasts and 8/151 *de novo* AML patients, emphasizing the rarity of these mutations in pediatric MDS ($P < 5.0 \times 10^{-6}$) and AML ($P < 0.02$) compared with adult cases. We found mutations in two JMML cases, JMML 4 and JMML 17. JMML 4 carried a heterozygous *U2AF35* mutation (R156M), whereas JMML 17 had a 6-bp in-frame deletion (c.518-523delAAGTCC) in *SRSF2* that resulted in deletion of amino acids S170 and K171 (Figure 1). Both nucleotide changes found in *U2AF35* and *SRSF2* were neither identified in the 60 healthy volunteers nor registered in the dbSNP database (<http://www.ncbi.nlm.nih.gov/projects/SNP/>) or in the 1000 genomes project, indicating that they represent novel spliceosome mutations in pediatric cases.

U2AF35 is the small subunit of the U2 auxiliary factor (*U2AF*), which binds an AG dinucleotide at the 3' splice site, and has an essential role in RNA splicing.¹³ With the exception of a single A26V mutation found in a case of refractory cytopenia with multilineage dysplasia, all the *U2AF35* mutations reported in adult myeloid malignancies involved one of the two hot spots within the two zinc-finger domains, S34 and Q157, which are highly conserved across species, suggesting the gain-of-function mutations.¹⁰ In JMML 4, the R156M *U2AF35* mutation affects a conserved amino acid adjacent to Q157, suggesting it may also be a gain-of-function mutation, leading to aberrant pre-mRNA splicing possibly in a dominant fashion.

SRSF2, better known as SC35, is a member of the serine/arginine-rich (SR) family of proteins.¹⁴ *SRSF2* binds to a splicing-enhancer element in pre-mRNA and has a crucial role not only in constitutive and alternative pre-mRNA splicing but also in transcription elongation and genomic stability.¹⁴ All mutations thus far identified in adult cases exclusively involved P95 within the intervening sequence between the N-terminal RNA-binding domain and the C-terminal RS domain.¹⁰ This region interacts with other SR proteins, again suggesting that the P95 mutation may result in gain-of-function.¹⁰ This proline residue is thought to determine the relative orientation of the two flanking domains of *SRSF2*, and a substitution at this position could compromise critical interactions with other splicing factors necessary for RNA splicing to take place. In contrast, the newly identified 6-bp in-frame deletion in JMML 17 results in two conserved amino acids, S170 and K171, within the RS domain. Although it may affect protein–protein interactions, the functional significance of this deletion remains elusive.

JMML is a unique form of pediatric MDS/MPN characterized by activation of the RAS/mitogen-activated protein kinase signaling pathway; in 90% of cases, there are germ line and/or somatic mutations of *NF1*, *NRAS*, *KRAS*, *PTPN11* and *CBL*.⁸ Although JMML shares some clinical and molecular features with CMML, its spectrum of gene mutations suggests that it is a neoplasm distinct from CMML.¹⁵ This was also confirmed by the current results that the splicing-pathway mutations are rare in JMML, whereas they are extremely frequent (~60%) in CMML.¹⁰ Although the two JMML cases carrying the splicing-pathway mutations had no known RAS-pathway mutations, both the pathway mutations frequently coexisted in CMML.⁸

To summarize, no mutations of *SF3B1*, *U2AF35*, *ZRSR2* or *SRSF2* are found in pediatric MDS and AML. In our study, except for *ZRSR2*, mutations were examined focusing on the reported hot spots in adult studies, raising a possibility that we may have missed some mutations occurring in other regions. However,

these hot spots represent evolutionally conserved amino acids and have functional relevance, it is unlikely that the distribution of hot spots in children significantly differs from adult cases and as such, we could safely conclude that mutations of *SF3B1*, *U2AF35*, *ZRSR2* and *SRSF2* are rare in myeloid neoplasms in children. Finally, mutations of *U2AF35* and *SRSF2* may have some role in the pathogenesis of JMML, although further evaluations are required.

CONFLICT OF INTEREST

The authors declare no conflict of interest.

ACKNOWLEDGEMENTS

This work was supported by Research on Measures for Intractable Diseases, Health and Labor Sciences Research Grants, Ministry of Health, Labor and Welfare, by Research on Health Sciences focusing on Drug Innovation, and the Japan Health Sciences Foundation. We would like to thank M Matsumura, M Yin, N Hoshino and S Saito for their excellent technical assistance.

J Takita^{1,2}, K Yoshida³, M Sanada³, R Nishimura¹, J Okubo¹,
A Motomura¹, M Hiwatari¹, K Oki¹, T Igarashi¹,
Y Hayashi⁴ and S Ogawa³

¹Department of Pediatrics, Graduate School of Medicine,
The University of Tokyo, Tokyo, Japan;

²Department of Cell Therapy and Transplantation Medicine,
Graduate School of Medicine, The University of Tokyo, Tokyo, Japan;

³Cancer Genomics Project, Graduate School of Medicine,
The University of Tokyo, Tokyo, Japan and


⁴Gunma Children's Medical Center, Gunma, Japan
E-mail: sogawa-tky@umin.ac.jp

REFERENCES

- García-Manero G. Myelodysplastic syndromes: 2011 update on diagnosis, risk-stratification, and management. *Am J Hematol* 2011; **86**: 490–498.
- Delhommeau F, Dupont S, Della Valle V, James C, Trannoy S, Masse A et al. Mutation in TET2 in myeloid cancers. *N Engl J Med* 2009; **360**: 2289–2301.
- Thol F, Friesen I, Damm F, Yun H, Weissinger EM, Krauter J et al. Prognostic significance of ASXL1 mutations in patients with myelodysplastic syndromes. *J Clin Oncol* 2011; **29**: 2499–2506.
- Ley TJ, Ding L, Walter MJ, McLellan MD, Lamprecht T, Larson DE et al. DNMT3A mutations in acute myeloid leukemia. *N Engl J Med* 2010; **363**: 2424–2433.
- Nikolovski G, Langemeijer SM, Kuiper RP, Knops R, Masson M, Tonnissen ER et al. Somatic mutations of the histone methyltransferase gene EZH2 in myelodysplastic syndromes. *Nature Genet* 2010; **42**: 665–667.
- Green A, Beer P. Somatic mutations of IDH1 and IDH2 in the leukemic transformation of myeloproliferative neoplasms. *N Engl J Med* 2010; **362**: 369–370.
- Sanada M, Suzuki T, Shih LY, Otsu M, Kato M, Yamazaki S et al. Gain-of-function of mutated C-CBL tumour suppressor in myeloid neoplasms. *Nature* 2009; **460**: 904–908.
- Perez B, Kosmider O, Cassinat B, Renneville A, Lachenaud J, Kaltenbach S et al. Genetic typing of CBL, ASXL1, RUNX1, TET2 and JAK2 in juvenile myelomonocytic leukaemia reveals a genetic profile distinct from chronic myelomonocytic leukaemia. *Br J Haematol* 2010; **151**: 460–468.
- Oki K, Takita J, Hiwatari M, Nishimura R, Sanada M, Okubo J et al. IDH1 and IDH2 mutations are rare in pediatric myeloid malignancies. *Leukemia* 2011; **25**: 382–384.
- Yoshida K, Sanada M, Shiraishi Y, Nowak D, Nagata Y, Yamamoto R et al. Frequent pathway mutations of splicing machinery in myelodysplasia. *Nature* 2011; **478**: 64–69.
- Chen Y, Takita J, Hiwatari M, Igarashi T, Hanada R, Kikuchi A et al. Mutations of the PTPN11 and RAS genes in rhabdomyosarcoma and pediatric hematological malignancies. *Genes Chromosomes Cancer* 2006; **45**: 583–591.
- Shiba N, Kato M, Park MJ, Sanada M, Ito E, Fukushima K et al. CBL mutations in juvenile myelomonocytic leukemia and pediatric myelodysplastic syndrome. *Leukemia* 2010; **24**: 1090–1092.

- 13 Zhang M, Zamore PD, Carmo-Fonseca M, Lamond AI, Green MR. Cloning and intracellular localization of the U2 small nuclear ribonucleoprotein auxiliary factor small subunit. *Proc Natl Acad Sci USA* 1992; **89**: 8769–8773.
- 14 Edmond V, Brambilla C, Brambilla E, Gazzeri S, Eymin B. SRSF2 is required for sodium butyrate-mediated p21(WAF1) induction and premature senescence in human lung carcinoma cell lines. *Cell Cycle* 2011; **10**: 1968–1977.

- 15 Emanuel PD. Juvenile myelomonocytic leukemia and chronic myelomonocytic leukemia. *Leukemia* 2008; **22**: 1335–1342.

 This work is licensed under the Creative Commons Attribution-NonCommercial-No Derivative Works 3.0 Unported License. To view a copy of this license, visit <http://creativecommons.org/licenses/by-nc-nd/3.0/>

Supplementary Information accompanies the paper on the Leukemia website (<http://www.nature.com/leu>)

Sequencing histone-modifying enzymes identifies UTX mutations in acute lymphoblastic leukemia

Leukemia (2012) **26**, 1881–1883; doi:10.1038/leu.2012.56

Mutations affecting epigenetic regulators have long been known to have a crucial role in cancer and, in particular, hematological malignancies.^{1,2} One of the earliest epigenetic factors described altered in leukemia was the mixed lineage leukemia (*MLL*) protein which is found translocated in 10% of adult acute myeloid leukemia (AML), 30% of secondary AML and >75% of infants with both AML and acute lymphocytic leukemia (ALL). *MLL* is a SET domain-containing protein, which is recruited to many promoters and mediates histone 3 lysine 4 (H3K4) methyltransferase activity, thought to promote gene expression.³

In addition to *MLL* fusions, recently, somatic mutations of *UTX* (also known as *KDM6A*), encoding an H3K27 demethylase, were described in multiple hematological malignancies, including multiple myeloma and many types of leukemia cell lines.^{4,5} H3K27 methylation is generally thought to cause gene repression. Complementary to *UTX*, mutations of *EZH2*, a H3K27 methyltransferase, have been reported in both lymphoid and myeloid tumors (Figure 1).^{6,7} These mutations lead to altered *EZH2* activity and influence H3K27 in tumor cells. Mutations in *EZH2*, *EED* and *SUZ12*, which all cooperate in Polycomb repressive complex 2 have been recently described in early T-cell precursor ALL.⁸ Similarly, point mutations affecting the functional jumonji C (jmc) domain of *UTX* inactivates its H3K27 demethylase activity. In addition, *UTX* associates with *MLL2* in a multiprotein complex, which promotes H3K4 methylation, and recently *MLL2* has also been found mutated in cancer, further pointing to a common and complex epigenetic deregulation in cancer.⁹ In line with the growing evidence for epigenetic regulators as important in tumorigenesis, additional mutations affecting epigenetic regulators such as *SETD2*, a H3K36 methyltransferase, *KDM3B*, a H3K9 demethylase, and *KDM5C*, a H3K4 demethylase, have been reported and are associated with distinct gene expression patterns (Figure 1).⁴

Though the clinical significance of these findings remains to be explored, it is evident that epigenetic deregulation is having an important role in both lymphoid and myeloid leukemogenesis. Furthermore, with novel drugs at hand, such as histone deacetylase inhibitors or demethylating agents that can target and reverse epigenetic alterations, understanding the underlying molecular aberrations is of growing interest.¹⁰ We therefore undertook an effort to examine the prevalence of somatic mutations in genes encoding histone-modifying proteins, in particular, *KDM3B*, *KDM5C*, *UTX*, *MLL2*, *EZH2* and *SETD2*, which previously were reported mutated in cancer.^{4,5}

For an initial screen, we analyzed banked diagnostic primary leukemia samples from 44 childhood B-cell ALL and 50 adult

AML patients, and, where available, used bone marrow samples obtained in complete remission to validate the somatic nature of the mutations. Samples had been collected with patient/parental informed consent from patients enrolled on Dana–Farber Cancer Institute protocols for childhood ALL (DFCI 00-001 (NCT00165178), DFCI 05-001 (NCT00400946)) or AML treatment protocols of the German–Austrian AML Study Group (AMLSG) for younger adults (AMLSG-HD98A (NCT00146120), AMLSG 07-04 (NCT00151242)), and the study was approved by the IRB of the participating centers.

Using conventional Sanger sequencing of primary leukemia sample-derived genomic DNA, we first screened all coding exons in which mutations have been reported previously.^{4,5} Initially, we analyzed a total of 36 of 174 exons (*KDM3B* (2/24), *KDM5C* (9/26), *UTX* (7/29), *MLL2* (8/54), *EZH2* (1/20) and *SETD2* (9/21)) and found 7 non-synonymous tumor-specific aberrations. In AML, we found one *EZH2* mutation (p.G648E) in a t(8;21)-positive, and two *MLL2* missense mutations (p.R5153Q and p.Y5216S; Table 1) and one

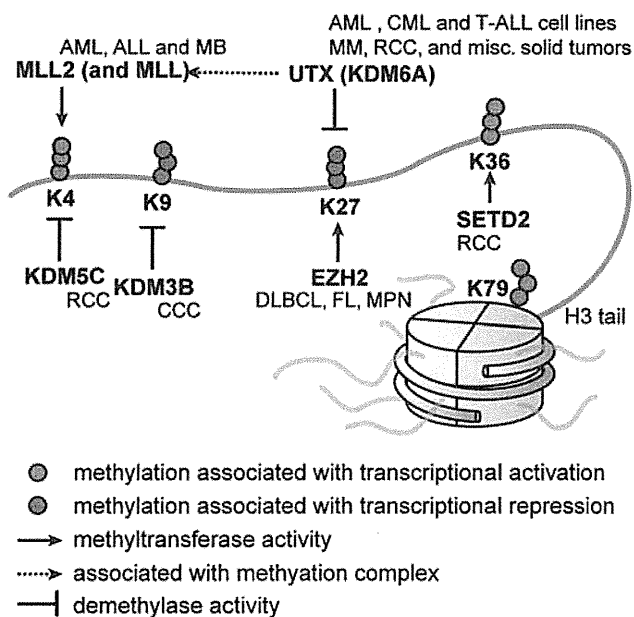


Figure 1. Histone 3 methylation and selected histone demethylases and methyltransferases. Cancers are shown in italics next to the mutated protein they are associated with. MM, multiple myeloma; FL, follicular lymphoma; DLBCL, diffuse large B-cell lymphoma; RCC, renal cell carcinoma; CCC clear cell carcinoma; MPN, myeloproliferative neoplasm; MB, medulloblastoma.

available at www.sciencedirect.com
journal homepage: www.europeanurology.com



Urothelial Cancer

Methylation of a Panel of MicroRNA Genes Is a Novel Biomarker for Detection of Bladder Cancer

Takashi Shimizu^{a,b}, Hiromu Suzuki^{b,c,*}, Masanori Nojima^{c,d}, Hiroshi Kitamura^a, Eiichiro Yamamoto^{b,c}, Reo Maruyama^{b,c}, Masami Ashida^b, Tomo Hatahira^b, Masahiro Kai^b, Naoya Masumori^a, Takashi Tokino^e, Kohzoh Imai^f, Taiji Tsukamoto^{a,**}, Minoru Toyota^b

^a Department of Urology, Sapporo Medical University, Sapporo, Japan; ^b Department of Molecular Biology, Sapporo Medical University, Sapporo, Japan; ^c First Department of Internal Medicine, Sapporo Medical University, Sapporo, Japan; ^d Department of Public Health, Sapporo Medical University, Sapporo, Japan; ^e Medical Genome Science, Research Institute for Frontier Medicine, Sapporo Medical University, Sapporo, Japan; ^f Division of Novel Therapy for Cancer, The Advanced Clinical Research Center, The Institute of Medical Science, The University of Tokyo, Tokyo, Japan

Article info

Article history:

Accepted November 13, 2012

Published online ahead of print on November 23, 2012

Keywords:

Biomarker
Bladder cancer
DNA methylation
MicroRNA
Urinary test

Abstract

Background: Dysregulation of microRNAs (miRNAs) has been implicated in bladder cancer (BCa), although the mechanism is not fully understood.

Objective: We aimed to explore the involvement of epigenetic alteration of miRNA expression in BCa.

Design, setting, and participants: Two BCa cell lines (T24 and UM-UC-3) were treated with 5-aza-2'-deoxycytidine (5-aza-dC) and 4-phenylbutyric acid (PBA), after which their miRNA expression profiles were analyzed using a TaqMan array (Life Technologies, Carlsbad, CA, USA). Bisulfite pyrosequencing was used to assess miRNA gene methylation in 5 cancer cell lines, 83 primary tumors, and 120 preoperative and 47 postoperative urine samples.

Outcome measurements and statistical analysis: Receiver operating characteristic (ROC) curve analysis was used to assess the diagnostic performance of the miRNA gene panel.

Results and limitations: Of 664 miRNAs examined, 146 were upregulated by 5-aza-dC plus PBA. CpG islands were identified in the proximal upstream of 23 miRNA genes, and 12 of those were hypermethylated in cell lines. Among them, miR-137, miR-124-2, miR-124-3, and miR-9-3 were frequently and tumor-specifically methylated in primary cancers (miR-137: 68.7%; miR-124-2: 50.6%; miR-124-3: 65.1%; miR-9-3: 45.8%). Methylation of the same four miRNAs in urine specimens enabled BCa detection with 81% sensitivity and 89% specificity; the area under the ROC curve was 0.916. Ectopic expression of silenced miRNAs in BCa cells suppressed growth and cell invasion.

Conclusions: Our results indicate that epigenetic silencing of miRNA genes may be involved in the development of BCa and that methylation of miRNA genes could be a useful biomarker for cancer detection.

© 2012 European Association of Urology. Published by Elsevier B.V. All rights reserved.

* Corresponding author. Department of Molecular Biology, Sapporo Medical University, S1, W17, Chuo-Ku, Sapporo 060-8556, Japan. Tel. +81 11 611 2111; Fax: +81 11 622 1918.

** Corresponding author. Department of Urology, Sapporo Medical University, S1, W16, Chuo-Ku, Sapporo 060-8543, Japan. Tel. +81 11 611 2111; Fax: +81 11 612 2709.

E-mail addresses: hsuzuki@sapmed.ac.jp (H. Suzuki), taijit@sapmed.ac.jp (T. Tsukamoto).

1. Introduction

MicroRNAs (miRNAs) are a group of small noncoding RNAs that negatively regulate the translation and stability of partially complementary target mRNAs. In that way, they play important roles in a wide array of biologic processes, including cell proliferation, differentiation, and apoptosis [1]. Increasing evidence suggests that dysregulation of miRNA expression contributes to the initiation and progression of human cancer [2,3]. Altered miRNA expression is thought to play an important role in the pathogenesis of bladder cancer (BCa) and in certain tumor phenotypes. For instance, high-grade BCa exhibits upregulation of several miRNAs, including miR-21, which suppresses p53 function [4]. In addition, miR-21-to-miR-205 expression ratios are elevated in invasive BCa cells [5], while miR-200 family members regulate epithelial-to-mesenchymal transition by targeting transcription repressors ZEB1 and ZEB2 in BCa cells [6].

Although the mechanisms underlying miRNA dysregulation in cancer are not yet fully understood, recent studies have shown that the silencing of several miRNAs is tightly linked to epigenetic mechanisms, including histone modification and DNA methylation [7,8]. For example, treatment with a histone deacetylase (HDAC) inhibitor and a DNA methyltransferase (DNMT) inhibitor restored expression of various miRNAs in cancer cells [7,9], and the list of miRNA genes methylated in cancer is rapidly growing [10]. Studies have also shown that restoration of epigenetically silenced miRNAs may be an effective strategy for treating cancer and that aberrant methylation of miRNA genes could be a useful biomarker for cancer detection [10,11]. In addition, it was recently shown that the silencing of miRNA expression in BCa is associated with DNA methylation, often involving the CpG island (CGI) or CpG shore [12,13]. In an effort to identify novel biomarkers and treatment targets in BCa, we aimed to identify miRNAs epigenetically silenced in BCa cells by screening for miRNAs whose expression is upregulated by DNA demethylation and HDAC inhibition. We also investigated the methylation of miRNA genes in urine specimens and assessed its clinical usefulness as a biomarker for detection of BCa.

2. Materials and methods

2.1. Cell lines and tissue samples

BCa cell lines (T24, UM-UC-3, HT-1197, HT-1376, SW780, and 5637) and a normal urothelial cell line (SV-HUC-1) were obtained from the American Type Culture Collection (ATCC, Manassas, VA, USA; Supplementary Table 1). A colorectal cancer cell line HCT116 harboring genetic disruptions within the DNMT1 and DNMT3B loci (DNMTs KO) have been described previously [8]. T24 and UM-UC-3 cells were treated first with 1 μ M or 0.1 μ M 5-aza-2'-deoxycytidine (5-aza-dC; Sigma-Aldrich, St Louis, MO, USA) for 72 h, and then with 3 mM 4-phenylbutyric acid (PBA; an HDAC inhibitor, Sigma-Aldrich) for 72 h, replacing the drug and medium every 24 h. A total of 83 primary BCa specimens were collected from patients who underwent radical cystectomy (RC) or transurethral resection of bladder tumor (TURBT; 66 males and 17 females; median age: 72 yr; range: 34–90 yr). Of the 83 patients, 73 underwent surgical

resection after initial diagnosis, 7 received chemotherapy before surgery, and 3 are recurrent cases. Samples of nontumorous bladder tissue adjacent (<2 cm) to and distant (>2 cm) from the tumors were also collected. Six samples of normal urothelial tissue from renal cell carcinoma (RCC) patients who underwent nephrectomy were also collected. Informed consent was obtained from all patients before collection of the specimens, and this study was approved by the institutional review board. Total RNA was extracted using a *mirVana* miRNA isolation kit (Life technologies, Carlsbad, CA, USA). Genomic DNA was extracted using the standard phenol-chloroform procedure.

2.2. Urine samples

Voided urine specimens were collected from 20 cancer-free individuals (Supplementary Table 2) and 86 BCa patients. In addition, postoperative voided urine samples were collected from 36 of the 86 patients 3–10 d after TURBT treatment. As an independent test set, preoperative urine samples were collected from 34 BCa patients, and postoperative samples were collected from 11 patients. The postoperative urine samples were collected from patients in whom tumors were successfully resected without leaving residual tumors. The urine (10 ml) was mixed with 5 ml of ThinPrep PreservCyt solution (Hologic, Bedford, MA, USA) and stored at 4 °C. Each sample was centrifuged at 3000 rpm for 10 min, and genomic DNA was extracted from the pelleted sediment using the standard phenol-chloroform procedure.

2.3. MicroRNA expression profiling

Expression of 664 miRNAs was analyzed using a TaqMan MicroRNA array v2.0 (Life Technologies). Briefly, 1 μ g of total RNA was reverse-transcribed using a Megaplex Pools kit (Applied Biosystems, Foster City, CA, USA), after which miRNAs were amplified and detected using polymerase chain reaction (PCR) with specific primers and TaqMan probes. U48 snRNA (RNU48, Life Technologies) served as an endogenous control.

2.4. Quantitative real-time polymerase chain reaction of miRNA

Expression of selected miRNAs was analyzed using TaqMan microRNA assays. Briefly, 5 ng of total RNA were reverse-transcribed using specific stem-loop real-time primers, after which they were amplified and detected using PCR with specific primers and TaqMan probes. U6 snRNA (RNU6B, Life Technologies) served as an endogenous control.

2.5. Methylation analysis

Bisulfite conversion of genomic DNA, methylation-specific PCR (MSP), bisulfite sequencing, and bisulfite pyrosequencing were carried out as described previously [8]. Primer sequences and PCR product sizes are listed in Supplementary Table 3. Primer locations for methylation analysis are shown in Supplementary Figure 1.

2.6. Transfection of microRNA precursor molecules

BCa cells (1×10^6 cells) were transfected with 100 pmol of Pre-miR miRNA Precursor Molecules (Life Technologies) or Pre-miR miRNA Molecules Negative Control #1 using a Cell Line Nucleofector kit R (Lonza, Basel, Switzerland) with a Nucleofector I electroporation device (Lonza) according to the manufacturer's instructions. The viability of the miRNA precursor transfectants was analyzed using water-soluble tetrazolium salt (WST) assays [8]. Cell invasion was assessed using Matrigel invasion assays [8].

2.7. Gene expression microarray analysis

One-color microarray-based gene expression analysis was carried out according to the manufacturer's instructions (Agilent Technologies, Santa Clara, CA, USA). Briefly, 100 ng of total RNA were amplified and labeled using a Low-input Quick AmpLabeling Kit One-color (Agilent Technologies), after which the synthesized cRNA was hybridized to a SurePrint G3 Human GE microarray (G4851F; Agilent Technologies). The microarray data were then analyzed using GeneSpring GX version 11 (Agilent Technologies). The Gene Expression Omnibus accession number for the miRNA microarray data is GSE41760.

2.8. Statistical analysis

All data were analyzed using GraphPad Prism 4.0 statistical software (GraphPad Software, La Jolla, CA, USA). Quantitative variables were analyzed using a Student *t* test and one-way analysis of variance (ANOVA) with a post hoc Tukey test. Fisher exact test was used for analysis of categorical data. The Pearson correlation coefficient was used to evaluate correlations between continuous data. Receiver operating characteristic (ROC) curves for the diagnosis of BCa were constructed on the basis of the methylation levels, followed by calculation of the area under the curve (AUC). The best cut-off value for each miRNA gene was defined as the point on the ROC curve closest to the upper left corner. A diagnostic scoring system using urinary DNA methylation was constructed by analyzing the training set using the following three-step algorithm: (1) The methylation status of miRNA genes was assessed using the respective cut-off values; (2) the number of methylation-positive genes was determined, which we termed the *miR-methylation score* (M-score); and (3) the samples were classified into five groups based on the M-score. The value of *p* < 0.05 (two-sided) was regarded as significant.

3. Results

3.1. Identification of epigenetically silenced microRNA genes in bladder cancer

To identify epigenetically silenced miRNAs in BCa, we performed TaqMan array analysis using two BCa cell lines (T24 and UM-UC-3) treated with 1 μM 5-aza-dC plus 3 mM PBA. Of the 664 miRNAs examined, the drug treatment induced upregulation (more than five-fold) of 208 miRNAs in T24 cells and 200 miRNAs in UM-UC-3 cells. Of those, 146 miRNAs were upregulated in both cell lines (Supplementary Fig. 2 and 3; Supplementary Table 4). We selected 23 miRNA genes that harbored CGIs in the proximal upstream (<5 kb) of their coding regions (Supplementary Table 5), and subsequent MSP analysis revealed that the CGIs of 12 were hypermethylated in multiple BCa cell lines (Fig. 1A). These miRNAs were also induced by a low dose (0.1 μM) of 5-aza-dC plus PBA, making it unlikely that the observed induction was a secondary effect of DNA damage (Supplementary Fig. 4).

We next used bisulfite pyrosequencing to quantitatively analyze the methylation of the 12 miRNA genes showing CGI methylation in a series of BCa tissues (*n* = 26), a sample of normal urothelium tissue, and a normal urothelial cell line (SV-HUC-1). We found that four miRNA genes (miR-137, miR124-2, miR-124-3, and miR-9-3) were frequently methylated in primary tumors, though their methylation levels were limited in normal urothelium (Fig. 1B; Supplementary Fig. 5 and 6). In addition, we observed a marked

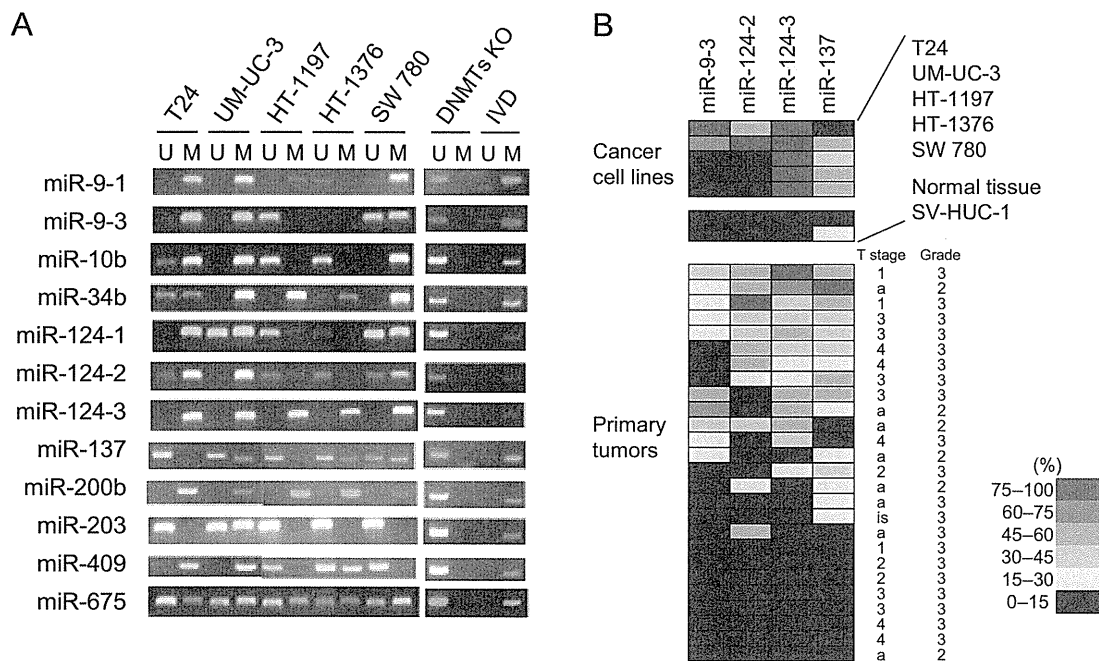


Fig. 1 – Methylation analysis of microRNA (miRNA) genes in bladder cancer (BCa). (A) Methylation-specific polymerase chain reaction (PCR) analysis of the CpG islands of 12 miRNA genes in the indicated cell lines. In vitro methylated DNA and DNA methyltransferase knockout cells served as positive and negative controls, respectively. Bands in the “M” lanes are PCR products obtained with methylation-specific primers; those in the “U” lanes are products obtained with unmethylated-specific primers. (B) Summarized results for the bisulfite pyrosequencing of miRNA genes in BCa cell lines, a sample of normal urothelial tissue, a normal urothelial cell line SV-HUC-1, and a set of primary BCa tissues (*n* = 26). Tumor stages and grades are indicated on the right.

DNMTs KO = DNA methyltransferase knockout cells; IVD = in vitro methylated DNA.

Table 1 – Correlation between microRNA gene methylation and the clinicopathologic features of bladder cancer

	(n = 83)	miR-137 met (%)			miR-124-2 met (%)			miR-124-3 met (%)			miR-9-3 met (%)		
		Mean	SD	<i>p</i> *	Mean	SD	<i>p</i> *	Mean	SD	<i>p</i> *	Mean	SD	<i>p</i> *
Age, yr:													
Median (range)	72 (34–90)	–	–	0.394	–	–	0.277	–	–	0.147	–	–	0.065
Gender:													
Male	66	26.7	19.9	–	25.1	23.9	–	32.0	24.4	–	19.8	17.4	–
Female	17	34.6	22.1	0.160	22.2	11.1	0.630	31.8	20.6	0.974	17.3	13.0	0.591
T stage:													
Ta	35	31.3	23.4	–	25.1	22.1	–	29.7	25.2	–	21.0	18.5	–
Tis	4	23.5	19.7	–	24.6	28.8	–	22.5	15.4	–	12.7	4.4	–
T1	8	33.4	19.2	–	33.9	29.9	–	42.6	25.2	–	24.9	16.2	–
≥T2	36	24.9	17.8	0.486	21.8	19.3	0.575	32.7	22.1	0.458	17.0	15.3	0.463
Grade:													
1	1	15.3	–	–	1.9	–	–	5.8	–	–	11.2	–	–
2	27	29.3	23.4	–	21.3	18.9	–	28.6	24.6	–	21.3	16.6	–
3	55	28.1	19.3	0.795	26.5	23.2	0.360	34.1	22.9	0.331	18.4	16.8	0.676
LN metastasis:													
N0	73	28.6	21.0	–	24.9	22.4	–	32.4	24.0	–	20.1	17.3	–
N1–N3	10	26.7	17.8	0.782	21.8	18.2	0.685	28.3	20.5	0.605	13.3	7.3	0.231

SD = standard deviation; LN = lymph node; ANOVA = analysis of variance.

* Pearson correlation coefficient, student *t* test, or ANOVA.

reduction in the methylation levels in BCa cells treated with 5-aza-dC plus PBA, which is consistent with the upregulation of miRNAs (Supplementary Fig. 7).

3.2. Methylation of microRNA genes in primary bladder cancer

We next examined the methylation levels of miR-137, miR-124-2, miR-124-3, and miR-9-3 in a larger set of primary tumors ($n = 83$), along with adjacent and distant nontumorous bladder tissues from the same patients (Table 1). Elevated levels of miRNA gene methylation ($>15.0\%$) were frequently detected in primary BCa tissues (miR-137: 57 of 83, 68.7%; miR-124-2: 42 of 83, 50.6%; miR-124-3: 54 of 83, 65.1%; miR-9-3: 38 of 83, 45.8%), and the tumor tissues exhibited significantly higher methylation levels than their nontumorous counterparts (Fig. 2A). In addition, we found that levels of miRNA gene methylation were more frequently elevated in adjacent nontumorous bladder tissues (AN; miR-137: 26 of 74, 35.1%; miR-124-2: 19 of 74, 25.7%; miR-124-3: 15 of 74, 20.3%; miR-9-3: 12 of 74, 16.2%) than in more distant nontumorous tissues (DN; miR-137: 18 of 83, 21.7%; miR-124-2: 6 of 83, 7.2%; miR-124-3: 11 of 83, 13.3%; miR-9-3: 9 of 83, 10.8%). No significant correlation was found between the levels of miRNA gene methylation and the clinicopathologic characteristics of the patients (Table 1).

When we examined the methylation status of miR-137 in selected tissue specimens in more detail, we observed dense methylation in tumor tissues but only scattered methylation in nontumorous tissues (Fig. 2B). We then compared the levels of miR-137 expression determined in TaqMan assays with the methylation levels obtained by bisulfite pyrosequencing in selected pairs of tumors and corresponding distant nontumorous tissues (Fig. 2C). We found that there was an inverse relationship between the expression of miR-137 and its methylation, which suggests

that CGI methylation is associated with the downregulation of miR-137 in BCa tissues.

3.3. Detection of microRNA gene methylation in urine samples

To assess the usefulness of miRNA gene methylation, we collected voided urine specimens from 86 BCa patients (Table 2) and 20 cancer-free individuals. Upon performing bisulfite pyrosequencing, we observed elevated methylation of miR-137, miR-124-2, miR-124-3, and miR-9-3 in the urine samples from the cancer patients (Fig. 3A) but only limited methylation of the genes in cancer-free individuals (Fig. 3B). Moreover, the methylation levels in the urine samples correlated positively with those in the corresponding tumor tissues (Supplementary Fig. 8). Notably, when we then collected postoperative voided urine samples from 36 of the 86 patients after surgical resection of their tumors, we observed dramatically reduced methylation levels (Fig. 3A; Supplementary Fig. 9).

To further evaluate the clinical usefulness of the miRNA gene methylation in urine samples, we carried out ROC curve analysis to assess its ability to distinguish preoperative from postoperative samples (Fig. 3C). The most discriminating cut-offs for miR-137, miR-124-2, miR-124-3, and miR-9-3 were 5.2% (sensitivity, 77.9%; specificity, 77.8%), 5.2% (sensitivity, 69.8%; specificity, 88.9%), 12.0% (sensitivity, 65.1%; specificity, 97.2%), and 7.2% (sensitivity, 69.4%; specificity, 86.1%), respectively (Table 3). We next compared these results with those obtained with urine cytology. Based on the urinary cytology using Papanicolaou's classification of the 86 patients, 55 (64%) were diagnosed as class I or II, 15 (17%) were class III, and only 16 (19%) were class IV or V (strongly suggestive or conclusive of malignancy), suggesting that the sensitivity of urinary methylation for detection of BCa is significantly greater than that of conventional cytology (Supplementary Table 6).

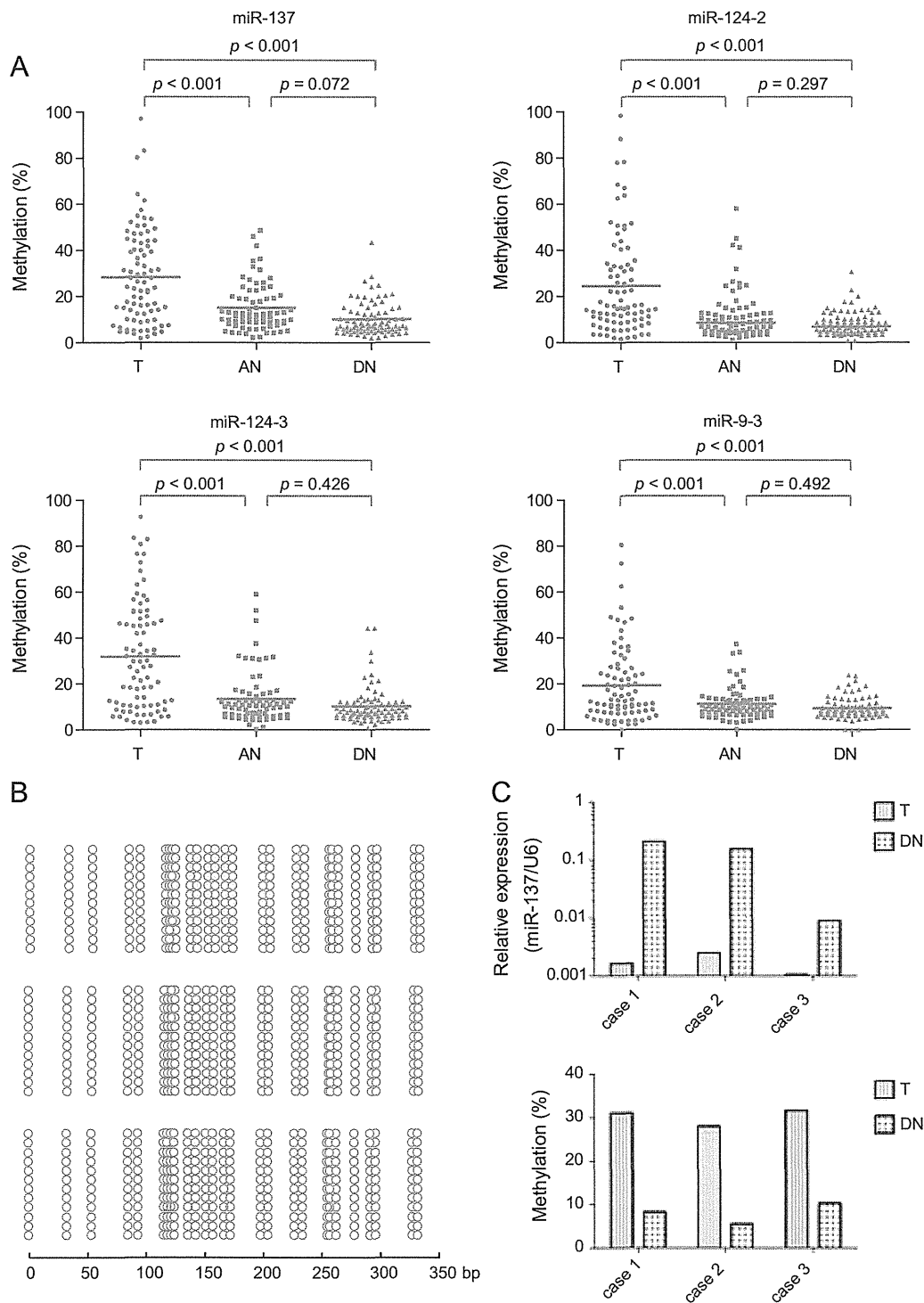


Fig. 2 – Analysis of microRNA (miRNA) gene methylation in primary bladder cancer. (A) Summarized results of bisulfite pyrosequencing of the indicated miRNA genes in primary tumors (T; $n = 83$), nontumorous bladder tissues adjacent to the tumors (AN; $n = 74$), and nontumorous bladder tissues distant from the tumors (DN; $n = 83$). $p < 0.05$. (B) Bisulfite sequencing analysis of the miR-137 CpG island (CGI) in a pair of tumor (T) and distant nontumorous tissues (DN). (C) Inverse relationship between the expression and methylation of miR-137 in three pairs of tumor (T) and distant nontumorous tissues (DN). Expression was assessed in TaqMan assays (upper panel), and methylation was determined by bisulfite pyrosequencing (lower panel).

To develop a more efficient diagnostic method for detecting BCa, we constructed a scoring system using the urinary methylation of the four methylated miRNA genes (Fig. 4). Using the cut-off value for each gene (Table 3), we classified the samples into five groups based on the

M-score. A ROC curve was then constructed to evaluate the ability of the scoring system to distinguish preoperative from postoperative urine samples by plotting the sensitivity over 1-specificity at each point (Fig. 4B). We then validated the diagnostic system by analyzing an independent test set

Table 2 – Clinicopathologic characteristics of the patients in the training and test sets

	Training set (n = 86)	Test set (n = 34)
Age, yr:		
Median (range)	73 (42–90)	71 (58–93)
Gender, no.:		
Male	69	25
Female	17	9
T stage, no.:		
Ta	34	16
Tis	7	5
T1	12	8
≥T2	33	5
Grade, no.:		
1	1	0
2	28	14
3	57	20
Lymph node metastasis, no.:		
N0	81	32
N1–N3	5	2
Treatment, no.:		
TURBT	64	30
RC	22	4

TURBT = transurethral resection of bladder tumor; RC = radical cystectomy.

(Table 2). AUCs in both sets were high (training set: 0.916; test set: 0.910), confirming the accuracy of our system for detecting BCa using urinary miRNA gene methylation (Fig. 4). We also found that our scoring system could effectively detect early-stage Ta and low-grade (grades 1 and 2) BCa (sensitivity: 0.679; specificity: 0.889; AUC = 0.862), which was undetectable using urinary cytology (Supplementary Fig. 10).

3.4. Functional analysis of microRNAs

To test whether any of the miRNAs could act as tumor suppressors, we transfected BCa cells with an miRNA precursor molecule or a negative control, and then carried out cell viability assays. The assays showed that ectopic expression of miR-137 or miR-124 suppressed BCa cell

proliferation, whereas miR-9 exerted no significant suppressive effect on growth (Supplementary Fig. 11 and 12). We then carried out Matrigel invasion assays to test the effect of the miRNAs on cell invasion. Although we detected no effect of miR-137 and miR-124 on cell invasion, ectopic expression of miR-9 suppressed the invasiveness of BCa cells (Supplementary Fig. 13).

Finally, to further clarify the effect of miRNAs, we carried out a gene expression microarray analysis of SW780 cells transfected with a miR-137 precursor or a negative control. We found that 1326 probe sets (1016 unique genes) were downregulated (more than two-fold) by ectopic miR-137 expression, including the previously reported miR-137 target genes cyclin-dependent kinase 6 (*CDK6*), cell division cycle 42 (*CDC42*), and aurora kinase A (*AURKA*) [14,15]. Among the 1016 downregulated genes, the TargetScan program predicted that 144 genes are potential targets of miR-137 (Supplementary Table 7). Moreover, Gene Ontology analysis revealed that genes related to the cell cycle were significantly enriched among the affected genes (Supplementary Table 8). Our results strongly suggest that the miRNAs in question act as tumor suppressors in BCa.

4. Discussion

We identified four miRNA genes (miR-137, miR-124-2, miR-124-3, and miR-9-3) that were frequently methylated in both cultured and primary BCa cells. Earlier studies have shown that these miRNAs are tumor-suppressive or tumor-related and that they are epigenetically silenced in cancers of various origins. Hypermethylation of miR-137 was first discovered in oral cancer [16] and has since been noted in other malignancies, including cancers of the colon [14] and stomach [3]. Within cancer cells, miR-137 targets *CDK6*, *CDC42*, and *AURKA*, which is indicative of its tumor-suppressive properties [14–16], whereas in normal cells, miR-137 regulates neuronal differentiation through targeting enhancer of zeste homolog 2 (*EZH2*) and mindbomb E3 ubiquitin protein ligase 1 (*MIB1*) [17,18]. Methylation of miR-124 family genes (miR-124-1, miR-124-2, and miR-124-3) was identified in colorectal cancer [19] and was also

Table 3 – Receiver operating characteristic analysis of microRNA gene methylation to detect bladder cancer

Gene name	Cut-off, %	Training set		
		AUC (95% CI)	Sensitivity (95% CI)	Specificity (95% CI)
miR-137	5.2	0.782 (0.701–0.862)	77.91 (67.67–86.14)	77.78 (60.85–89.88)
miR-124-2	5.2	0.769 (0.686–0.851)	69.77 (58.92–79.21)	88.89 (73.94–96.89)
miR-124-3	12.0	0.805 (0.730–0.880)	65.12 (54.08–75.08)	97.22 (85.47–99.93)
miR-9-3	7.2	0.778 (0.697–0.860)	69.41 (58.47–78.95)	86.11 (70.50–95.33)
Gene name	Cut-off, %	Test set		
		AUC (95% CI)	Sensitivity (95% CI)	Specificity (95% CI)
miR-137	5.2	0.816 (0.693–0.938)	79.41 (62.10–91.30)	63.64 (30.79–89.07)
miR-124-2	5.2	0.866 (0.758–0.975)	79.41 (62.10–91.30)	90.91 (58.72–99.77)
miR-124-3	12.0	0.901 (0.807–0.995)	58.82 (40.70–75.35)	100.0 (71.51–100.0)
miR-9-3	7.2	0.797 (0.660–0.934)	76.47 (58.83–89.25)	72.73 (39.03–93.98)

AUC = area under the curve; CI = confidence interval.

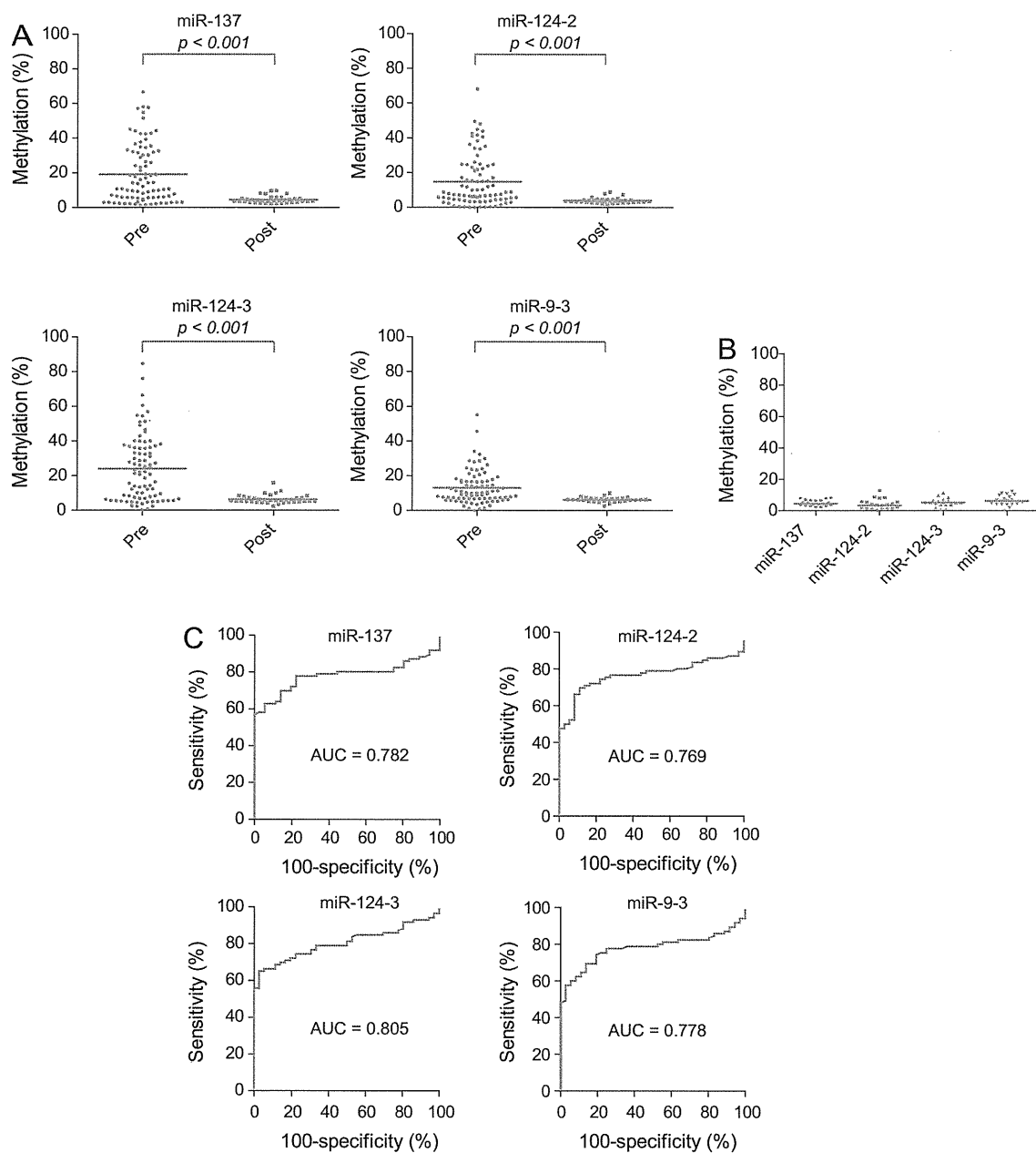


Fig. 3 – Detection of microRNA (miRNA) gene methylation in urine specimens from bladder cancer (BCa) patients. (A) Summary of bisulfite pyrosequencing analysis of the indicated miRNA genes in voided urine samples collected from BCa patients before (Pre: $n = 86$) and after surgical treatment (Post: $n = 36$). $p < 0.001$. (B) Bisulfite pyrosequencing results for miR-137, miR-124-2, miR-124-3, and miR-9-3 in voided urine samples from cancer-free individuals ($n = 20$). (C) Receiver operating characteristics curve analysis of the ability of miRNA gene methylation to distinguish preoperative and postoperative urine samples. AUC = area under the curve.

found in gastric cancer [20], hematologic malignancies [21], and hepatocellular carcinoma [22]. In addition, screening for methylated miRNA genes in metastatic cancer cell lines also identified miR-9 family genes (miR-9-1, miR-9-2, and miR-9-3) [23].

Cumulative evidence suggests that miRNAs play important roles in the pathogenesis of BCa, and previous studies demonstrated their epigenetic silencing in the disease. For example, miR-34a, which is a direct target of p53 and a candidate tumor suppressor gene, is frequently methylated and silenced in many types of cancer, including BCa [24]. In

addition, Wiklund et al. found that the silencing of miR-200 family genes and miR-205 is associated with DNA methylation in invasive BCa [12]. They also showed that reduced expression of miR-200c is associated with disease progression and poor outcome, suggesting that epigenetic silencing of miR-200 family genes could be a prognostic marker in BCa. Recently, Dudzic et al. carried out an miRNA microarray analysis after treating normal urothelium and urothelial cancer cell lines with 5-azacytidine. They identified 4 mirtrons and 16 miRNAs whose silencing was associated with DNA methylation [13]. Some of those

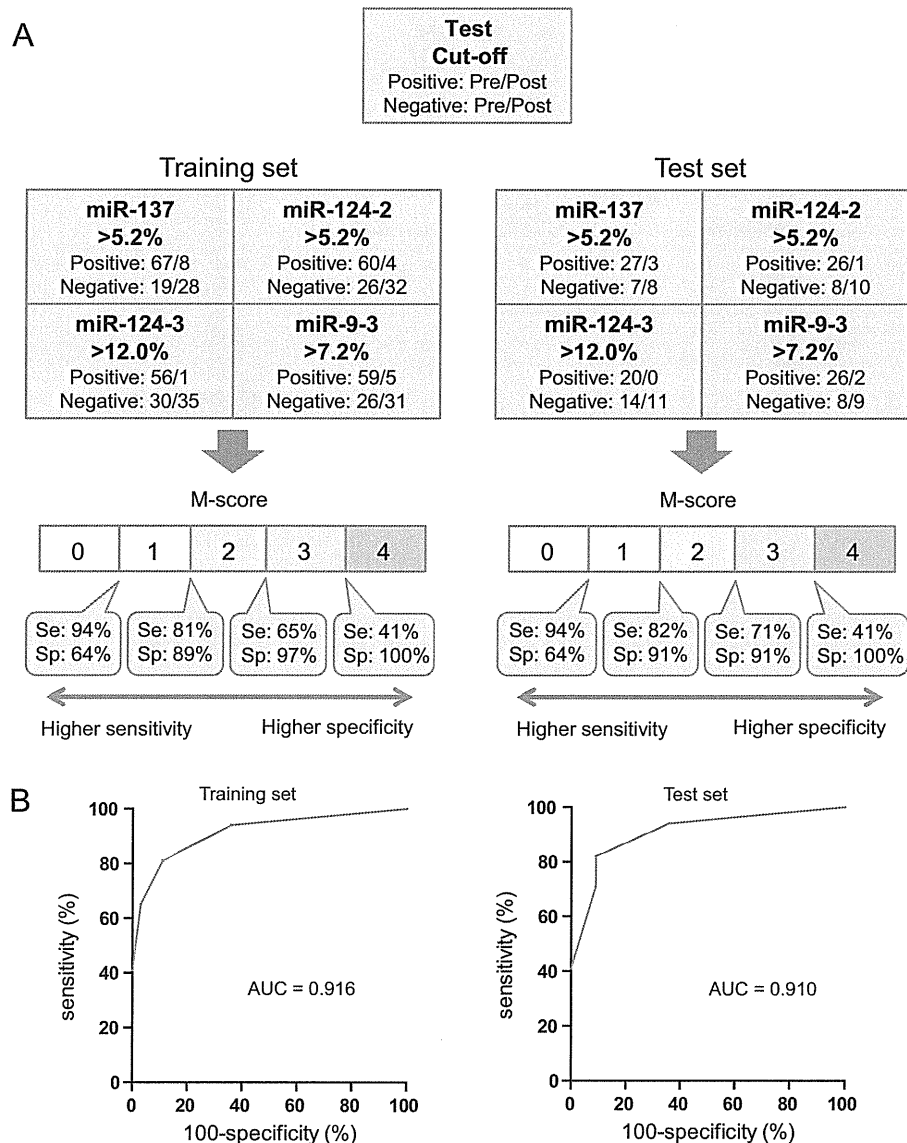


Fig. 4 – Diagnostic system for detecting bladder cancer (BCa) using urinary microRNA (miRNA) gene methylation. (A) Workflow of a system established based on the ability to distinguish preoperative from postoperative urine. Results of the training set are shown on the left; those of test set are on the right. The methylation status of miRNA genes in preoperative (training set: $n = 86$; test set: $n = 36$) and postoperative urine (training set: $n = 34$; test set: $n = 11$) was determined using the cut-off values in the respective boxes. A miR-methylation score (M-score) was determined from the number of methylation-positive genes, and samples were classified into five groups based on the M-score. The sensitivity (Se) and specificity (Sp) at each point are indicated below. (B) Receiver operating characteristic curve analysis of the training and test sets. Areas under the curve are shown in the graph. M-score = miR-methylation score; AUC = area under the curve.

mirtrons and miRNAs, including miR-9 family genes, more frequently exhibited CpG shore methylation than CGI methylation, suggesting that methylation in both the CpG shore and CGI is related to epigenetic silencing of miRNA in BCa. Interestingly, miR-9-1 and -9-2 were associated with both CGI and CpG shore methylation, whereas miR-9-3 showed only CGI methylation [13]. Consistent with those findings, we observed that among the miR-9 family genes, miR-9-3 most frequently showed CGI methylation.

Methylation of several miRNA genes is strongly related to the clinical characteristics of cancer, suggesting its potential usefulness as a biomarker. For instance, methylation of miR-9-1 and -9-3 is reportedly associated with metastatic recurrence of RCC, which is indicative of the

possible role of miR-9 in cancer metastasis [25]. Despite this report, however, we did not find a significant difference in the levels of miR-9-3 methylation between noninvasive and invasive BCa tissues. Further study to clarify the functions of these miRNAs in BCa will be needed.

Recent studies have shown that miRNA levels in urine could serve as a molecular marker for detection of BCa. For instance, expression of miR-96 and miR-183 is reportedly upregulated in urothelial cancer, and their detection in urine strongly distinguished cancer patients from cancer-free patients [26]. Miah et al. also showed that evaluation of a panel of 10 miRNAs in urine is a highly sensitive method of detecting BCa [27]. DNA methylation is another potential molecular marker detectable in urine specimens. Several